The Cryosphere
Discussions

Glacial sedimentation, fluxes and erosion rates associated with ice retreat in Petermann Fjord and Nares Strait, NW Greenland

Kelly A. Hogan[1,2], Martin Jakobsson[3,4], Larry Mayer[2], Brendan Reilly[5], Anne Jennings[6], Alan Mix[5], Tove Nielsen[7], Katrine J. Andresen[8], Egon Nørmark[8], Katrien A. Heirman[7,9], Elina Kamla[7,10], Kevin Jerram[2],
Christian Stranne[3,4]

[1] British Antarctic Survey, Natural Environment Research Council, High Cross, Madingley Road, Cambridge, CB3 0ET, UK
[2] Center for Coastal and Ocean Mapping, University of New Hampshire, Durham, NH 03824, USA
[3] Department of Geological Sciences, Stockholm University, 106 91 Stockholm, Sweden
[4] Bolin Centre for Climate Research, Stockholm University, 106 91 Stockholm, Sweden
[5] College of Earth, Ocean, and Atmospheric Sciences, Oregon State University, Corvallis, OR 97331, USA
[6] Institute of Arctic and Alpine Research, University of Colorado, Boulder, CO 80309-0450, USA
[7] Geological Survey of Denmark and Greenland, Øster Voldgade 10, 1350 Copenhagen K, Denmark
[8] Department of Geoscience, Aarhus University, Hoegh-Guldbergs Gade 2, DK-8000, Aarhus C, Denmark
[9] TNO, Geological Survey of the Netherlands, Princetonlaan 6, NL-3584 CB Utrecht, The Netherlands
[10] Rambøll Management Consulting, Hannemanns Allé 53, DK-2300 Copenhagen S, Denmark

Correspondence to: Kelly Hogan (kelgan@bas.ac.uk)

Abstract. Petermann Fjord is a deep (>1000 m) fjord that incises the coastline of northwest Greenland and was carved by an expanded Petermann Glacier, one of the six largest outlet glaciers draining the modern Greenland Ice Sheet (GrIS). Between 5-70 m of unconsolidated glacigenic material infills in the fjord and adjacent Nares Strait, deposited as the Petermann and Nares Strait ice streams retreated through the area after the Last Glacial Maximum. We have investigated the deglacial deposits using seismic stratigraphic techniques and have correlated our results with high-resolution bathymetric data and core lithofacies. We identify six seismo-acoustic facies in more than 3500 line-km of sub-bottom and seismic-reflection profiles throughout the fjord, Hall Basin and Kennedy Channel. Seismo-acoustic facies relate to: bedrock or till surfaces (*Facies I*); subglacial deposition (*Facies II*); deposition from meltwater plumes and icebergs in quiescent glaciomarine conditions (*Facies III, IV*); deposition at grounded ice margins during stillstands in retreat (grounding-zone wedges; *Facies V*); and the redeposition of material down slopes (*Facies IV*). These sediment units represent the total volume of glacial sediment delivered to the mapped marine environment during retreat. We calculate a glacial sediment flux for the former Petermann Ice Stream as 1080-1420 m³ a⁻¹ per meter of ice stream width and an average deglacial erosion rate for the basin of 0.29-0.34 mm a⁻¹. Our deglacial erosion rates are consistent with results from Antarctic Peninsula fjord systems but are several times lower than values for other modern GrIS catchments. This difference is attributed to fact that large volumes of surface water do not access the bed in the Petermann system and we conclude that glacial erosion is limited to areas overridden by streaming ice in this large outlet glacier setting. Erosion rates are also presented for two phases of ice retreat and confirm that there is significant

35 variation in these rates over a glacial-deglacial transition. Our new fluxes and erosion rates show that the Petermann Ice Stream was approximately as efficient as the palaeo-Jakobshavn Isbrae at eroding, transporting and delivering sediment to its margin during early deglaciation.

1 Introduction

40 Fjords act as important repositories for glacial-marine sediments deposited by retreating glaciers because once a marine-terminating glacier has its grounded margin within a fjord, any sediments expelled from it are often effectively trapped in the narrow basin setting. In addition, fjord geometry strongly influences glacier retreat behaviour because bathymetric sills, fjord constrictions and turns in the fjord planform shape all provide stability either by reducing the flux at the grounding line and/or by providing lateral buttressing (Warren and Hulton, 1990; Hill et al., 2018; Åkesson et al., 2018; Catania et al., 2018).

45 Furthermore, the grain size and distribution of sedimentary deposits delivered to the marine environment from an ice margin are related to the processes of ice-mass loss (iceberg calving versus melt; e.g., Andresen et al., 2012; Witus et al., 2014; Simkins et al., 2017). Discrete deposits (grounding-zone wedges, terminal moraines) also record phases of ice-margin stability (e.g., Alley et al., 1986; Larter et al., 1994; Powell, 2002). This is significant because it means that variations in the types, volumes and architecture of glacial-marine sediment delivered to fjords reflect both ice-dynamic processes and mass-loss mechanisms

50 during retreat. There can also be a sediment record produced during glacier advance (e.g., surges; Elverhøi et al., 1983; Gilbert et al., 2002) but these are less relevant when looking for analogues for the rates and modes of modern glacial retreat. Thus, investigations of the sediment infill of fjords provide an important tool for reconstructing past changes in glacier behaviour as well as palaeoenvironmental conditions across the glacier drainage area.

Many such studies exist for Norwegian and Svalbard fjords; however, in Greenland, ship-based research is hampered by

55 difficult ice conditions and relatively remote locations, issues that generally increase in complexity further north. Fjords housing major outlet glaciers are often choked by an ice mélange – a dense pack of calved icebergs and sea ice (cf. Amundsen et al., 2010) – that render some fjords almost inaccessible to research vessels. This situation is augmented in northern Greenland by persistent sea-ice cover cementing icebergs together in winter and extending far beyond the coast for up to 11 months of the year (DMI, 2018). As a result, there are only a few previous studies of marine sediments from northern Greenland (e.g.,

60 Jennings et al., 2011, 2019; Madaj, 2016; Reilly et al., *In press*), and none with extensive or detailed geophysical mapping of the glacial sediment infill in fjords. This was remedied by the *Petermann 2015 Expedition*, which collected, in addition to terrestrial, biological and oceanographic datasets (Münchow et al., 2016; Heuzé et al., 2017; Lomac-MacNair et al., 2018), a comprehensive suite of marine geophysical and geological data from Petermann Fjord and the adjacent part of Nares Strait, northwest Greenland (Jakobsson et al., 2018). Combining systematic classification and mapping of the seismic (acoustic)

65 datasets with seafloor geomorphology provides a means to correlate sediment infill with glacidynamic processes leading to an

The Cryosphere
Discussions
Open Access
EGU

improved understanding of the Holocene retreat of the Petermann and Nares Strait ice streams (cf. England, 1999; Jakobsson et al., 2018).

This study reconstructs de- and post-glacial sedimentary processes and fluxes in Petermann Fjord and the adjacent stretch of Nares Strait using seismic stratigraphy and seismo-acoustic facies. The objectives are: (1) to describe and interpret seismo-

70   acoustic facies from sub-bottom and seismic-reflection profiles; (2) to map unlithified sediment units and calculate the volumes of glacigenic deposits; (3) to determine glacial sediment fluxes to Nares Strait and Petermann Fjord for known stillstands during deglaciation; (4) to calculate glacial erosion rates for the Petermann ice stream catchment during deglaciation; and (5) to provide geological boundary conditions for numerical glacier modelling exercises. This is the first comprehensive study of the sediment stratigraphy in the fjord beyond a major Greenland outlet glacier and the first from the northern part of the

75   landmass. It sheds new light on the rates of sediment delivery to the margins of Greenland's outlet glaciers and the rates of glacial erosion that generated this sediment during glacial retreat. Glacial sediment fluxes and erosion rates are rare for Greenland; our estimates can be compared with other areas but also provide direct observational constraints on future numerical modelling efforts.

2 Regional setting

80   ### 2.1 Environmental setting (geology, physiography, oceanography)

Nares Strait is the narrow body of water between northwest Greenland and Ellesmere Island that opens out northwards in to the Lincoln Sea and Arctic Ocean (Fig. 1). The northern part of the strait consists of Robeson Channel, Hall Basin and Kennedy Channel, and is typically around 30 km wide, 400-800 m deep. Kennedy and Robeson channels have generally smooth seafloors, however Hall Basin is somewhat wider (~40-60 km) and has a notably rougher or fractured seafloor beyond the

85   mouth of Petermann Fjord (Jakobsson et al., 2018; Fig. 2). The bedrock geology in the area consists of Precambrian basement rocks capped by Paleozoic platform limestones that have been dissected by two sets of approximately orthogonal faults trending NNE-SSW and N-S. The Wegener Transform Fault, which crosses from Judge Daly Promontory to Kap Lupton (Fig. 2) in the study area but extends northwards in Nares Strait (Dawes 2004; Tessensohn et al., 2006), provides a strong structural control on seafloor morphology in Hall Basin (Jakobsson et al., 2018).

90   Petermann Fjord is a deep (>1000 m), relatively flat-bottomed fjord with a straight planform shape that is 15-20 km wide. The fjord walls have steep gradients (>70°) resulting in a box-like cross-section. The most prominent bathymetric feature of the fjord is a sill at the fjord-mouth rising to between 350-450 m water depth but with its deepest part (443 m) about 2 km west of the midline of the fjord mouth (Jakobsson et al., 2018). Modified Atlantic Water flows into both Nares Strait and Petermann Fjord from the Lincoln Sea (Münchow et al., 2016; Johnson et al., 2011) but is overlain by a cooler, fresher water mass (Arctic

95   Water) that is also advected in to the fjord (Straneo et al., 2012). Oceanographic results from the *Petermann 2015 Expedition* have shown that water in the fjord is dominated by Atlantic Water at depth (450-600 m) which does not interact with the 40-km long floating ice tongue over the fjord, but is thought to reach the grounding line resulting in melting there (Münchow et

al., 2016; Heuzé et al., 2017). Meltwater from Petermann Glacier was also recorded in all 46 hydrographic casts collected in 2015 in the fjord and in Nares Strait, with meltwater exiting the fjord on its northern side at water depths of 100-300 m (Heuzé et al., 2017). The present-day retreat of Greenland's marine-terminating glaciers, including Petermann Glacier, has been partly attributed to warming of the Atlantic Water that reaches the ice margins and enhances frontal melting (Holland et al., 2008; Straneo et al., 2012; Rignot et al., 2012; Johnson et al., 2011; Heuze et al., 2017; Cai et al., 2017). Furthermore, AW was present in Hall Basin during deglaciation and may have promoted grounded ice retreat during deglaciation (Jennings et al., 2011).

2.2 Late Weichselian to Holocene glacial history

During the LGM the ice sheet in northern Greenland was coalescent with the Innuitian Ice Sheet over Ellesmere Island (England, 1999; England et al., 2006), and grounded ice occupied Nares Strait. The distribution and magnitude of isostatic rebound in the area suggests that ice was at least 1 km thick in Nares Strait and terrestrial landforms indicate that Greenland ice extended across to the eastern side of Ellesmere Island (England, 1999). Ice is thought to have been distributed northward and southward from Kane Basin in central Nares Strait, with deglaciation of the strait occurring from its northern and southern ends from 11.3 cal. ka BP and 11.7-11.2 cal. ka BP, respectively (recalibrated from England, 1999; Jennings et al., 2019). A sediment core from northeastern Hall Basin indicates that this area, in front of Petermann Fjord, was free from grounded ice by 9.7 cal. ka BP and was experiencing distal glaciomarine conditions by 8.9 cal. ka BP (Jennings et al., 2011). Further south, dates from a core in Kane Basin show that it had deglaciated around 9.0 cal. ka BP (Georgiadis et al., 2018). Owing to uncertainties in the reservoir corrections for the area and differences in the material dated for deglacial ages, there is still some debate as to when the ice saddle between northwest Greenland and Ellesmere Island disintegrated. However, a recent study by Jennings et al. (2019) discussed this issue in detail and concluded that the strait could have opened as early as 9.0 cal. ka BP or as late as 8.3 cal. ka BP.

Reconstructions of full-glacial ice flow in the area include northeastward flow out of Nares Strait contributing to eastward flow of ice along the north Greenland coastal plain (Möller et al., 2010; Larsen et al., 2010; Funder et al., 2011). North of Kane Basin, strong convergent flow from the Innuitian and Greenland ice sheets, as evidenced by glacial striae and erratics, probably resulted in an ice stream in Nares Strait (England et al., 2006). This flow pattern is supported by recent mapping of glacial lineations including mega-scale glacial lineations (MSGL) in Kennedy and Robeson channels which indicate northward movement of fast-flowing grounded ice in the strait, most likely representing the late deglacial imprint of grounded ice activity (Jakobsson et al., 2018). A change in lineation orientation close to the mouth of Petermann Fjord was interpreted as a signature of ice exiting the fjord and merging with ice flow in Nares Strait causing a slight deflection in the flow pattern (Jakobsson et al., 2018).

By combining terrestrial evidence with the submarine landform record, Jakobsson et al. (2018) suggested the following sequence of events for the deglaciation of northern Nares Strait and Petermann Fjord (Fig. 1b). All ages were inferred by correlating the mapped marine landforms to dated ice margins on land by England (1999). Since the ice margins on land were

presented as uncalibrated ^{14}C years BP (England, 1999), calibration to calendar years was made by Jakobsson et al. (2018) using the Marine13 radiocarbon age calibration curve (Reimer et al., 2013) and a $\Delta R = 268 \pm 82$ years.

At 9.3 cal. ka BP (1σ range: 9440-9140 cal. a BP) the retreating ice margin was grounded between Kap Lupton and the Judge Daly Promontory along a prominent bathymetric shoaling (S4 on Fig. 2). At this time, there is evidence for abundant

135   meltwater release and ice stagnation on the eastern side of Hall Basin. By 8.7 cal. ka BP (1σ range: 8835-8459 cal. a BP) the ice margin is thought to have retreated to the mouth of Petermann Fjord where it rested on the prominent fjord-mouth sill (Fig. 1b) and was probably fronted by an ice tongue. A significant sedimentary wedge – a grounding-zone wedge (GZW) – built up on the sill reinforced ice-margin stability at this location (cf. Alley et al., 2007; Dowdeswell and Fugelli, 2012). Sometime later, the ice margin lost its ice shelf and retreated down the backside of the sill as a tidewater glacier cliff due to catastrophic

140   calving by a process termed marine ice cliff instability (Pollard et al., 2015). Based on terrestrial dates this is inferred to have occurred around 7.6 cal. ka BP (1σ range: 7740-7495 cal. a BP), after which the retreat of grounded ice through the remainder of the fjord was rapid. Recent sedimentological work suggests that the fjord was probably not covered by a floating ice tongue directly after this rapid retreat of the grounded Peterman Ice Stream (which became Petermann Glacier), for around 5000 years in the mid-Holocene (Reilly et al., *In press*). The modern glaciologic setting, which includes a 40-km long floating tongue, did

145   not develop until c. 2.2 cal. ka BP (Reilly et al., *In press*).

3 Methods

3.1 Geophysical datasets

Two primary datasets were used in this study: high-resolution, sub-bottom profiles (SBP) and airgun seismic-reflection profiles (AG), both collected during the *Petermann 2015 Expedition* to the Petermann Fjord and Nares Strait area in 2015 on the

150   Icebreaker (IB) *Oden*. More than 3100 line-km of SBP were acquired using the hull-mounted parametric Kongsberg SBP 120, which transmits a low-frequency (2.5-7 kHz) chirp pulse with a narrow (3°) main beam. Vertical resolution of the SBP profiles is approximately 0.35 ms (~70 cm using a sediment velocity of 1500 m s^{-1}). Penetration was up to 60 m in unlithified sediments and the quality of the SBP data was generally good, although frequently influenced by noise from ice breaking. Two artefacts are prominent in the data: (i) on steep slopes, side echoes and the scattering of acoustic energy resulted in returned reflections

155   being diffuse, and (ii) a rugged and hard seafloor generated numerous sidewall echoes and hyperbolae. Line spacing was generally as low as 600 m and rarely exceeded 2.5 km (Fig. 1b). The multidisciplinary nature of the expedition required an abundance of sampling stations and, in turn, resulted in numerous crossing lines and multiple transects of key areas (Fig. 2). The nature of deeper sediments and bedrock structure were studied using 10 AG profiles (Fig. 2) acquired with a single airgun source (210 cu. in. Generator Injection (GI) gun with a firing interval of 5 s and a record length of 3 s). The streamer had a

160   total active length of 300 m with 48 hydrophone groups (8 hydrophones each) and was towed at depths of 7-16 m. Navigation for the SBP profiles was taken directly from the ship's Seatex Seapath 320 GPS feed. Motion correction of the SBP data was applied using information provided by the installed Seatex MRU5 motion reference unit. For the AG profiles, a separate Thales

DG16 GPS system was used to calculate positions and offset geometries for the ship, source, and hydrophones. Heritage seismic-reflection profiles acquired in 2001 were also available and were used to investigate the character of key glacial

165   landforms. These data were acquired by Bundesanstalt für Geowissenschaften und Rohstoffe (BGR) using 6 GI guns and a 48-channel array (24 hydrophones each) in a 100 m-long streamer (shortened due to ice conditions). Details of the acquisition and processing of this dataset (BGR lines on Fig. 2) are provided in Jackson et al. (2006).

Processing of the SBP data involved calculation of instantaneous amplitudes from the correlated SBP120 output which were then visualized as variable density traces in dgB Earth Sciences open-source software, OpendTect (v. 6.4.0). The 2015

170   AG profiles were processed using standard processing techniques including geometry definition, amplitude correction and bandpass filtering preserving data in the frequency range of 40-350 Hz. FK-filtering was applied in order to remove propeller noise. After CDP (common depth point) stacking and migration, a gentle trace mix and automatic scaling was also applied. The output AG data were interpreted in Petrel 2015 and OpendTect. The seismic datasets were analysed alongside a gridded 3D surface of the seafloor produced from multibeam-bathymetric data also acquired during the *Petermann 2015 Expedition*.

175   The bathymetric data were collected using a Kongsberg EM122 (12 kHz) multibeam echosounder in a 1° (TX) x 1° (RX) array. Data coverage and water depths in the area resulted in the final grid having 15 m square grid cells. Detailed information and interpretation of the multibeam bathymetric dataset is presented in Jakobsson et al. (2018).

3.2 Seismic data interpretation

All output profiles are in two-way travel time (TWT). Seismo-acoustic facies were identified primarily from SBP profiles

180   based on reflection geometry, reflection strength and continuity; these were cross-checked on AG profiles and one additional facies (IV) was identified only on AG profiles. For the SBP data, the profiles were inspected and a coherent and continuous, high-amplitude reflection (R1) at the base of the uppermost unlithified sediment package (often marking the acoustic basement) was identified and digitized (Figs. 3a, c). In general, this reflection was picked manually; auto-tracking methods in OpendTect could not be used due to the variable penetration of the SBP 120, the rugged nature of the reflection, the noise artefacts noted

185   above and some limitations with the 2D picking algorithm. R1 picks on SBP profiles were supplemented and verified by the deeper-penetrating AG lines (Figs. 3b, d). R1 picks were gridded to make 3D surfaces for two areas: Petermann Fjord and Nares Strait, based on the separation of these areas by the shallow sill at the fjord-mouth over which the unlithified sediments disappear (on SBP profiles), and the known glacial history of the area (see Section 2.2). Isopach maps for the unlithified sediment package were produced by subtracting the depth-converted R1 surface from the multibeam-bathymetric DEM of the

190   seafloor; in general, stratigraphic thicknesses in metres in this study have been calculated using a sediment sound velocity of 1500 m s^{-1} (cf. Nygård et al., 2007; Hjelstuen et al., 2009; Hogan et al., 2012). Key glacial landforms, in this case GZWs, were also identified and mapped on the AG and SBP data. Base GZW reflections were digitized where AG profiles exist over these features and where they were visible on SBP profiles. These were gridded (using the 'surface' splines in tension algorithm in GMT; Smith and Wessel, 1990), converted to depth below the seafloor, and used to calculate GZW volumes. For the GZWs,

195   volumes were calculated with sediment velocities of 1500 m s^{-1} but also with the higher value of 1800 m s^{-1}. The latter value

is based on previous estimates of velocities in subglacial tills from (over-ice) seismic data (e.g., Smith, 1997; Tulaczyk et al., 1998; King et al., 2004), including recent measurements from Greenland (Hofstede et al., 2018) and on the measured physical properties of coarse shelf sediments including diamictons (e.g., Hamilton, 1969; Cochrane et al., 1995). Thus, for GZW thicknesses and volumes a range of values is given.

200

4 Results and interpretation

4.1 Seismo-acoustic facies and depositional environments in Petermann Fjord and Nares Strait

We identify six seismo-acoustic facies in Petermann Fjord and the adjacent area of Nares Strait (Fig. 4) and correlate these with core lithologies where possible (Supp. Fig. 1). These are: (I) *Acoustically-impenetrable to homogenous facies.* This facies
205 is represented by a high-amplitude, prolonged reflection defining a rugged surface with rare sub-bottom point and diffraction hyperbolae on slopes. It marks the base of the acoustic stratigraphy on SBP profiles and we interpret it to be bedrock or a till surface. The SBP data alone does not allow us to differentiate between these two types, but by correlating with AG lines where seismic basement is reached we can identify this facies as bedrock in Hall Basin. However, in areas where glacial lineations (which are formed subglacially in deforming till) are present the upper reflection of this unit is interpreted to be a till surface
210 (e.g., Fig. 5b). (II) *Acoustically-homogenous, non-conformable facies.* This unit has a strong, prolonged upper reflection and a lower amplitude basal reflection that can be discontinuous. It is acoustically-homogenous and shows varying thickness that is not conformable with the basal reflection or underlying units. In areas where this unit is correlated with MSGL it is interpreted as a subglacial till layer (cf. Ó Cofaigh et al., 2005); where this unit occurs on seafloor highs in Nares Strait it is interpreted as an iceberg ploughed or current-reworked facies based on correlation with iceberg ploughmarks on the multibeam
215 bathymetry data. (III) *Acoustically-stratified, conformable facies.* This is characterized by parallel to sub-parallel, continuous, high- to medium-amplitude reflections with conformable geometries. It is typically 5-15 m thick. We interpret this facies as glaciomarine and/or hemipelagic sediments primarily deposited via suspension settling (with variable IRD) in an ice-distal setting. (IV) *Acoustically-stratified basin or onlapping fill.* This facies also comprises parallel to sub-parallel, continuous, high- to medium-amplitude reflections either in a ponded basin-fill geometry (reflections terminate at basin sides) or in an
220 onlapping fill geometry (reflections curve up the flanks of basins). It can include acoustically-transparent bodies, usually several meters thick, that pinch out laterally. This facies is interpreted as a combination of suspension settling of glaciomarine and hemipelagic sediments and gravity-flow deposits (GFDs) forming the acoustically-transparent bodies (see *Facies V*) made up of material redeposited into basins from nearby slopes. (V) *Acoustically-transparent facies.* Multiple reflectors in Kennedy Channel comprise this facies in lense-shaped or tapered bodies on slopes. This facies is also present in local basins where it
225 often pinches out towards the basin flanks, both in Petermann Fjord and Hall Basin. The lensoid and pinching-out geometries of these units, their erosion of underlying sediments, and their acoustically-transparent nature is characteristic of GFDs (cf. Laberg and Vorren, 2000; Hjelstuen et al., 2009). (VI) *Downlapping to chaotic facies.* This facies is only seen on the AG

profiles over the GZWs in the area. It consists of low-amplitude chaotic point reflections and rare discontinuous, sub-parallel reflections forming either a layered or downlapping pattern. The location of this facies at a known GZW location (Jakobsson

230   et al., 2018), and its seismic character, are consistent with its interpretation as subglacial till forming a GZW on a bathymetric high (e.g., Anderson, 1999; Dowdeswell and Fugelli, 2012). Deposition most likely occurred via subglacial plastering (aggradation) on the ice proximal slope of the wedge and via small gravity flows on the ice-distal slope. These processes probably occurred asynchronously with aggradation during advance of the grounding line over the sill and progradation only occurring when the grounding zone was on the sill. Thus, the GZW on the sill may be more of a combined morainal bank with

235   GZW on its upper part, rather than a wedge-shaped GZW in its traditional form.

4.2 Petermann Fjord

The deep part of Petermann Fjord, the fjord bottom, which lies inside of (SE of) the mouth sill within the steep sidewalls (up to 70° slopes), is generally draped by a 5-15 m thick acoustically-stratified unit (*Facies III*) (Figs. 5, 7). This unit conformably overlies an impenetrable, prolonged reflection defining a rugged surface (*Facies I*; Fig. 5). Sediment cores sampling this unit

240   (*Facies III*) show that it consists of clayey muds with dispersed sands and clasts interpreted as glaciomarine sediments deposited from meltwater plumes and as ice-rafted debris (IRD) (Supp. Fig. 1) (Reilly et al., *In press*). The seafloor morphology of the fjord bottom, which comprises relatively flat-lying parts separated by steep "steps" and has been strongly sculpted by ice (Jakobsson et al., 2018), suggests that the basal reflection here usually represents bedrock. In the few small areas where glacial lineations have been identified (e.g., around 61° 39'W, 81° 03.5' N) the basal reflection on SBP profiles represents a

245   subglacial till surface (Fig. 5b). On the terraces on the western side of the fjord, bedrock is covered by about 5 m of stratified, conformable drape (*Facies III*) overlying a thin, non-conformable, acoustically-homogenous unit (*Facies II*) interpreted as glaciomarine/hemipelagic sediment overlying a plastered till unit.

On the eastern side of the fjord and in some places in the mid-fjord area, about 25 km from the 2015 ice tongue margin, local basins in the bedrock surface are filled with at least 35 m of stratified sediments (Fig. 5c). This basin fill is typically

250   ponded in basins in the central part of the fjord, and has an onlapping geometry and more transparent sub-units in basins on the eastern side of the fjord (*Facies IV*; Supp. Fig. 1g). We interpret these both as glaciomarine/hemipelagic sediments with the onlapping fill including interbedded GFDs promoted by increased sediment input from two small glaciers entering the fjord there (Belgrade Glacier and Unnamed Glacier; Fig. 2). Some basins in the central fjord also contain sediment gravity flow deposits (Fig. 5b) presumably representing material redeposited from local slopes. From the seafloor morphology, we

255   note that there are two clear fan-shaped deposits in the fjord immediately seaward of the margins of Belgrade and Unnamed glaciers, which are interpreted as ice-proximal fans (e.g., Fig. 7). Unfortunately, the SBP profiles do not penetrate into the fan deposits and we do not have AG profiles in this area.

4.3 Nares Strait (Hall Basin, Kennedy Channel, Robeson Channel)

In Hall Basin, between the Petermann fjord-mouth sill and the S2 high (Fig. 2), the seafloor deepens to 500-620 m and includes

260   several small basins (1 to >10 km^2), sometimes interconnected and expressed as flat areas of seafloor interrupted by rugged seafloor highs. The highs are acoustically-impenetrable (*Facies I*), are variously ice sculpted (Jakobsson et al., 2018) and are easily interpreted as bedrock. In the basins, the unlithified sediment package consists of stratified basin fill with GFDs (*Facies IV*) up to 45 m thick. Between basins, bedrock is mantled by 10-15 m of acoustically-stratified, conformable units (*Facies III*). Together these units are interpreted to be the product of rainout of glaciomarine and hemipelagic material that forms

265   conformable layers over bedrock where slopes are relatively gentle, but is focused in to basins by redeposition from nearby slopes (gradients up to 20°). The largest flow deposits (GFDs) are apparent as thick (>10 m) acoustically-transparent bodies (Fig. 6) and indicate that redeposition from the basin sides is an important process locally. They are correlated with the flattest basin floors with sharp, well-defined basin edges showing that sediment has run in to the basin and then been dammed by a bedrock high (Fig. 6a). On the most prominent bedrock highs (S2-S4; Fig. 2), unlithified sediments have an acoustically-

270   homogenous character and variable thickness (*Facies II*) that is usually <8 m thick (Fig. 6b). However, in deeper areas (> 350 m water depth) the rugged bedrock surface is mantled with 7-15 m of conformable, acoustically-stratified sediment (*Facies III*; Fig. 6). We interpret this pattern to reflect a dominance of rainout processes that uniformly draped bedrock/till with up to 15 m of layered sediments unless: (i) material was redeposited down-slope and into basins, or (ii) strong currents in Nares Strait (e.g., Mudie et al., 2006; Münchow et al., 2006) prevented the deposition of fine-grained material on the highest seafloor

275   areas. Iceberg ploughing also probably helped to homogenize sediment layers deposited on the highs (cf. iceberg ploughmarks on S2 in Jakobsson et al., 2018).

In the >500 m deep and relatively flat Kennedy and Robeson channels, unconsolidated sediment comprises a two-layer stratigraphy with a conformable geometry (*Facies III*). The upper unit is acoustically-stratified and is typically 5-10 m thick. The lower unit, which is separated from the upper unit by a high-amplitude reflection (R1 in Fig. 3), is also 5-10 m thick and

280   conformable but can be either acoustically homogenous or acoustically stratified (e.g., *Facies III* on Fig. 4). Where the bottom unit is homogenous on SBP profiles it has a stratified character on AG lines (cf. Fig. 3). We interpret this as reflection of the SBP acoustic signal at R1 and, therefore, poor penetration of acoustic energy in to the bottom unit. MSGL in Kennedy Channel are formed in *Facies II* interpreted as a subglacial till. A similar interpretation is made for MSGL in Robeson Channel where the MSGL are also formed in *Facies II* but underlie 5-10 m of *Facies III* as described above.

4.4 Grounding-zone wedges (GZWs)

285

There are two GZWs in the study area, one on the Petermann fjord-mouth sill that was identified by Jakobsson et al. (2018) and one in Kennedy Channel around 64° 39' W, 81° 09' N identified in this work from the SBP data (Figs. 8, 9). Both of these features are well covered by SBP lines and the Petermann GZW is also crossed by four AG profiles.

SBP profiles across the Petermann GZW show very limited penetration through this deposit. It has a high-amplitude

290   reflection at its top and is otherwise acoustically-impenetrable (*Facies I*). Only small mounds of acoustically-homogenous

material occur above this reflection; these were interpreted as recessional moraines based on their coincidence with small,

sinuous ridges in the multibeam dataset (Supp. Fig. 3 in Jakobsson et al., 2018). AG profiles over the GZW provide some more

information about its internal character (Fig. 8c). The GZW appears to contain several conformable reflections in its upper 50

ms (~37-45 m) that down-lap at the base of the slope (Figs. 4, 8c, d); however, the reflections have low amplitudes and are

295   discontinuous. Below these reflections the seismic character is poorly defined and chaotic (*Facies VI*) presumably because the

deposit consists of a similar lithology throughout and, therefore, contains few acoustic impedance contrasts. However, the base

of the deposit can be mapped along about 50 % of its length (e.g. Fig. 8c, d) and defines a surprisingly thick deposit (200 ms

TWT; ~150-180 m) that is continuous down the back slope of the fjord-mouth sill. We interpret this seismo-acoustic facies to

be a diamictic deposit probably consisting of subglacial till plastered on to the sill by a formerly-expanded Petermann Glacier

300   (cf. Petermann Ice Stream in Jakobsson et al., 2018). Coarse grains in the till deposit result in strong scattering of acoustic

energy, making this deposit effectively impenetrable with the SBP source. It is notable that the GZW does not appear to contain

the prograding reflections described from some GZWs (e.g., Larter and Vanneste, 1995; Anderson, 1999; Dowdeswell and

Fugelli, 2012); we attribute this to its position on the back-slope and upper ridge of the fjord-mouth sill. In this setting, it is

difficult to see how a wedge would be built up by progradation up a slope (i.e., on the back-slope of the sill). The deposit has

305   instead been built by plastering of layers of material on the back-slope and possibly with progradation on the top of the sill.

The Kennedy Channel GZW has a different geometry, position and architecture (Fig. 9). The GZW rises 10-15 m from

the surrounding seafloor, is at least 5 km wide (along Kennedy Channel) and 7 km long (across Kennedy Channel). Although

the multibeam echosounder coverage extends only to the mid-line of the channel, we note that the strait gets shallower towards

Ellesmere Island in this area (based on our multibeam dataset and IBCAO regional bathymetry; Jakobsson et al., 2012),

310   meaning that the GZW persists across the deepest channel in the strait. It has a convex-up expression in the bathymetry that is

clearly marked by iceberg ploughmarks (Fig. 9a) and is situated in current water depths of ~450 m just south of a marked slope

to deeper waters (~530 m) to the north (Fig. 9a). SBP profiles reveal that the deposit comprises 1-3 acoustically-transparent

units with variable thicknesses demarked by weak sub-bottom reflections (*Facies V*; Figs 9c, d). AG lines in this area, which

do not extend across the mapped GZW and do not fully image the deposit (Fig. 9a), reveal a chaotic seismic character (*Facies*

315   *VI*) sometimes forming lenticular bodies. However, the deposit thins and eventually pinches-out to the north (Figs 9c, d). We

interpret this acoustic signature as layers of subglacial till deposited (probably by gravity flows) at the temporarily stabilized

grounding zone of the Nares Strait Ice Stream. The ice margin stabilized at a bathymetric shallowing and narrowing of the

deepest channel in this area. Subglacial till extruded from the grounding line as GFDs formed the acoustically-homogenous

units (*Facies V*) extending and tapering down-slope in front of the GZW (Fig. 9d). Where such flow deposits are prolific and

320   occur at the seafloor, they are easily identified as smooth, lobate features in front of known grounding-zone positions marked

by terminal moraines (e.g., Ottesen and Dowdeswell, 2006; Flink et al., 2015) or GZWs (e.g., Bjarnardóttir et al., 2013; Esteves

The Cryosphere
Discussions
Open Access
EGU

et al., 2017). Here, they may reflect local shifts in the location of the grounding zone during a phase of ice-shelf instability interpreted from core records (Jennings et al., 2018) prior to further grounding-zone retreat.

5 Sediment volumes

5.1 Unlithified sediments in Petermann Fjord and Hall Basin

Total sediment thicknesses (to acoustic basement) were mapped from SBP profiles in two areas: Petermann Fjord and inner Hall Basin (Fig. 10). The isopach map for Petermann Fjord indicates that sediment thicknesses, typically 20-40 m, are relatively consistent on the fjord bottom with a few depressions holding 70 m of sediment (Fig. 10a). The total mapped sediment volume in the fjord was 14.2 km^3. In Hall Basin, mapping was confined to the area in front of the Petermann sill and south of ridges S1-S3. This was primarily because the sill is a known grounding-zone location during ice retreat (Jakobsson et al., 2018) and because that area contains the majority of the sediment-filled basins in front of the sill and up to the topographic barrier at S2-S4. Secondary to this, the area beyond the S1-S3 ridges has a heavily fractured morphology with many small, isolated basins and trenches; these features complicate calculations of sediment thickness when survey lines have irregular spacing that is often greater than the distance between individual basins. However, mapping and the resultant isopach map for this area indicates sediment thicknesses are typically less than 30 m but up to 50 m in basins, which become more irregular in shape further northwards (Fig. 10b). The strong correlation of sediment thickness with seafloor morphology confirms that topography is a strong control on accumulation in this area. The total mapped sediment volume between the fjord-mouth and the S1-S3 ridges is 16.3 km^3 (using a sound velocity of 1500 m s^{-1}).

5.2 Unlithified sediments in GZWs

The isopach map for the Petermann GZW shows a maximum sediment thickness of 215-260 m on the upper part of the back-slope of the fjord-mouth sill (Fig. 8b). The thickest part of the deposit appears to be confined to a central fjord-parallel line, which is likely a function of gridding from a single line in the central part of the fjord (line 04a; Fig. 8a) and likely leads to an underestimation in sediment thicknesses for the GZW. However, a second line across the southern part of the sill (line 13b) confirms that the GZW does not extend off the top part of the sill in this area (Fig. 8b). Sediment thicknesses on the top of the sill are generally between 30-120 m but reach 160-190 m in its northern part. The shape of the GZW is defined by a zero-thickness contour as mapped on AG profiles joined by tracing along the front scarp of the wedge and extending down the deepest channel into Petermann Fjord. A volume calculation for the isopach map representing the GZW at mouth of the Petermann Fjord gives a total volume of 7.7-15.1 km^3 (using sound speeds of 1500 and 1800 m s^{-1}). In Kennedy Channel, AG profiles do not fully cover the GZW (Fig. 9a); however, its volume has been estimated based on AG profiles and from SBP profiles that image the base of the deposit near its edges. The deposit here is more classically wedge-shaped (cf. Alley et al., 1989; Dowdeswell and Fugelli, 2012) compared to the deposits of the GZW at the Petermann Fjord mouth. The Kennedy Channel wedge has the greatest thickness toward the centre of the channel in the frontal part of the wedge (65-78 m; Fig. 9b).

11

The total sediment volume for the mapped part of the wedge is 1.1-2.2 km^3; however, our data only covers about half the width of the channel and we recognize that the deposit could be larger.

6 Discussion

6.1 Glacial sediment infill, volumes and fluxes

Describing and interpreting the seismic stratigraphy of unlithified sediments in glacier-influenced settings provides the large-scale geometries of deposits that can then be related to glacial landforms observed in bathymetry datasets and with sediments directly sampled by seafloor coring (cf. Dowdeswell et al., 2016). In high-latitude fjords and glacial troughs beyond the coastline, the unlithified sediment accumulation may be taken to represent material deposited since these areas were last occupied by grounded ice, during ice retreat following the LGM (e.g., Aarseth, 1997; Gilbert et al., 1998; Hjelstuen et al., 2009; Hogan et al., 2012). This assumes that the areas were fully excavated (to bedrock) by grounded ice during the previous glacial event, although this may not always be the case. In those instances, older (pre-LGM) sediment can be preserved forming the lowermost part of the stratigraphy (e.g., Hooke and Elverhøi, 1996; Aarseth, 1997; O'Regan et al., 2017; Jennings et al., 2019). However, theoretical studies of glacial erosion/sediment transport that are based on observations most often suggest that fjords are rapidly and fully excavated during glacial advances (Powell, 1984; Aarseth, 1997; Hjelstuen et al., 2009). This assumption is generally accepted in studies of glacial erosion rates based on fjord sediment volumes (e.g., Powell, 1991; Hunter, 1994; Hallet et al., 1996) and we also apply it in this study. This assumption is motivated because we are not able to distinguish old pre-LGM sediments in our data. However, support for this is derived from the seafloor morphology of Petermann Fjord and Hall Basin where glacially-sculpted bedrock surfaces are clearly visible (Jakobsson et al., 2018) indicating that significant pre-LGM sediments most likely do not occur.

Glaciomarine sedimentation seaward of marine-terminating ice streams (or glaciers) has two components (Fig. 11). First, coarse or mixed material delivered to the grounding zone as subglacial deposits (dark grey on Fig. 11), and second, predominantly fine-grained units (with some coarser particles) that settle out from meltwater plumes within several tens of kilometers from the grounding line ("plumites"; Hesse et al., 1997; yellow on Fig. 11) and as IRD. Taken together these two components represent the total glacial sediment volume delivered to the marine margin of an outlet glacier or ice stream, and if the period of time over which delivery occurred is known then the glacial sediment flux can be calculated. Here, we have mapped the two glaciomarine sedimentary components for the Petermann Fjord-Nares Strait system from the deglacial seismic stratigraphy: the fine-grained sediment units (*Facies III-IV*) deposited in front of, but relatively close to (within several 10s of kms), a marine-terminating glacier margin plus the mixed-grain size sediments deposited close to the grounding zone (*Facies V, VI*). Therefore, from our mapping we are able to calculate the total volume of glacial sediment delivered by the Petermann Ice Stream during deglaciation, when it was located at the fjord mouth.

Adding the Petermann GZW volume (7.7-15.1 km^3) to the volume of unlithified sediments in inner Hall Basin (16.3 km^3) returns a total glacial sediment volume of 24-31.4 km^3. We elect to remove 0.5 m of sediment cover for the mapped area

385　in Hall Basin because dates from nearby sediment cores there reveal that the upper ~ 0.5 m of material was deposited after the ice margin had retreated in to the fjord (Jennings et al., 2011, 2018), and because we expect that at least some material in inner Hall Basin has come from ice grounded in Kennedy Channel. It is not yet known whether the GZW was produced over multiple glacial cycles so we assume, for the purposes of these calculations, that the entire GZW was deposited during the last glacial period. We also assume that other sediment sources (biogenic, aeolian, sidewall erosion) are volumetrically insignificant,

390　which is typically the case in polar fjord settings (Powell, 2005). This is supported by total organic carbon (TOC) measurements on core tops from the area that return extremely low percentages TOC (<<0.5 %) (Jennings, *pers. comm.*) and by the lack of widespread GFDs in the fjord or in Hall Basin (Figs. 5-7). The result is a total sediment volume of 23.8-31.2 km^3; if this volume was deposited over the ~1100 years when the ice margin was stable at the fjord mouth (England, 1999; Jakobsson et al., 2018), it indicates a glacial sediment flux for the Petermann Ice Stream of 1080-1420 m^3 a^{-1} m^{-1}. (The flux per year was

395　divided by a by grounding line length of 20 km measured along the wedge front multibeam bathymetry to get the flux per meter ice stream width). Using the 1σ uncertainties in ages for the Jakobsson et a. (2018) ice margin positions (maximum time at the fjord mouth 1340 yrs; minimum time at the fjord mouth 720 yrs) we can give the associated uncertainty in these fluxes as 890-2170 m^3 a^{-1} m^{-1}. However, we acknowledge the remaining uncertainties with these estimates due to the possibility that some material from the GZW was produced by a previous glacial event and also that some sediment may bypass the system

400　(Petermann Fjord and Hall Basin) in icebergs that melt out elsewhere; it is not possible to quantify these volumes based on currently available data.

　　This sediment flux is between estimates for modern ice streams (typically ~10^2 m^3 a^{-1} m^{-1}; Kamb, 2001; Englehardt and Kamb, 1998; Anandakrishnan et al., 2007; Christoffersen et al., 2010) and those for the largest Norwegian palaeo-ice streams that delivered sediment to the shelf break (6000-11000 m^3 a^{-1} m^{-1}; Nygard, 2003; Nygard et al., 2007). The calculated flux

405　range is notably similar to the range provided by Hogan et al. (2012) using the same methods for the palaeo-Jakobshavn Isbrae (1030-2300 m^3 a^{-1} m^{-1}) when that ice stream was also stable at its fjord-mouth sill, although that estimate did not include a subglacial (coarse/mixed grain) component. During the LGM, these two ice streams operated with the same glacier thermal regime (i.e., warm-based streaming ice; Roberts and Long, 2005; Ó Cofaigh et al., 2013; England, 1999; Jakobsson et al., 2018), which is known to be a primary control on glacial erosion rates along with climate (Hallet et al., 1996; Koppes et al.,

410　2015). These two factors dominate over other variables like ice cover, sliding speeds and even ice flux (Elverhøi et al., 1998; Koppes et al., 2015), which explains the comparable estimates despite the larger (albeit modern) ice discharge of Jakobshavn Isbrae compared to Petermann (cf. Rignot and Kanagaratnam, 2006; Enderlin et al., 2014). The nature of the substrate is also important when considering sediment fluxes (Hallet et al., 1996) but its effect is somewhat difficult to assess for the two systems. Jakobshavn Isbrae erodes in to banded gneiss with variable foliation and jointing (Roberts & Long, 2005) whereas

415　Petermann Fjord has been eroded into bedded limestones of lower Paleozoic age (Dawes et al., 2000) with slabs being removed along bedding planes. The bedrock steps left by removal of limestone beds are visible in the seafloor morphology (Fig. 2; Jakobsson et al., 2018). Upstream of the bedded limestones, the bedrock is the typical Archaean crystalline basement of Greenland that includes gneisses and granitoids (Henriksen et al., 2009). The abrasion strength of these rock types (based on

Schmidt hammer rebound values; Krabbendam and Glasser, 2011) are similar if the limestones are hard (Goudie, 2006) but

420 jointing is a major control on glacial plucking (e.g., Sugden et al., 1992; Dühnforth et al., 2010). Thus, it is difficult to distinguish between the erodability of bedded limestones and Archaean basement versus jointed gneiss. Numerical modelling of these systems over our mapped bedrock surfaces and replicating our glacial fluxes would elucidate which factors control subglacial erosion rates and transport in the Petermann system. However, given the comparability of the two glacier systems, it appears from our results that the Petermann Ice Stream was approximately as efficient as the palaeo-Jakobshavn Isbrae at

425 eroding, transporting and delivering sediment to its margin during the early deglaciation.

6.2 Glacial erosion rates

The physiography of Petermann Fjord – a straight, box-like basin with a bounding sill at the fjord-mouth – lends itself towards volumetric studies of sediment infill and glacial erosion because it is an efficient trap for glacially-sourced sediment. Indeed, previous work from other fjord systems confirms that if a fjord has certain characteristics, one being bounding bathymetric

430 sills, then most of the sediment that is delivered by tidewater glaciers remains in the fjord system (i.e., sediment bypass to the ocean does not occur; e.g. Powell & Molnia, 1989; Andrews et al., 1994; Gilbert et al., 1993). This assumption is particularly reasonable for Petermann because of its simple geometry, its prominent bathymetric fjord-mouth sill, and the presence of additional significant bathymetric highs within several tens of kilometers of the fjord mouth (S1-S4; Fig. 2) that presumably act to further prevent sediment bypass out of Hall Basin. In a recent study, Fernandez et al. (2016) used the volumes of glacial

435 sediment infill from eight Patagonian and Antarctic Peninsula fjords spanning the latitudinal range 46° to 65° S to calculate the most likely millennial-scale erosion rates for each system since the fjords were last glaciated. They then compared these to climatic parameters (T, precipitation) to test how erosion varied as a function of latitude. We apply the methodology outlined in Fernandez et al. (2016) to our volumetric results to calculate the average erosion rate ($\bar{E}$) for the (palaeo) Petermann basin during its retreat from the fjord mouth. The total volume of glaciomarine sediment delivered by the palaeo Petermann Ice

440 Stream is the volume of Hall Basin and GZW sediment (23.8-31.2 km^3) plus the unconsolidated sediment in the fjord (14.2 km^3). Using a wet density of 1850 kg m^{-3} (based on measured density values from *Petermann 2015 Expedition* cores) for the sediments (ρ_{sed}) and a density of 2700 kg m^{-3} for the source rocks (ρ_{source}) (a commonly used density for parental rock types gneiss and limestones; following Andrews et al., 1994 and Fernandez et al., 2016) this total volume (38-45.4 km^3) was converted to a rock-equivalent volume of 26-31.1 km^3. After Fernandez et al., the basin- and time-averaged erosion rate can

445 then be calculated through:

$$\bar{E} = Vol_{Rx} / (A_{dr} \text{ x } T) \tag{1}$$

where A_{dr} is the effective drainage basin area (10 493 km^2) and T is the time for sediment accumulation (T), in effect the time

450 since grounded ice had retreated from the fjord-mouth sill (8700 years). This returns an average deglacial erosion rate of 0.29-0.34 mm a^{-1}. For the palaeo-Petermann catchment we note that its area could not be significantly larger than the modern

drainage basin because the ice stream was constrained to the fjord during deglaciation and the grounding line was at the fjord-mouth sill. Thus, we simply add the deglaciated area of the fjord to the modern Petermann catchment where ice velocities are high enough to allow glacial erosion and transport (i.e., where ice is at the pressure melting point and is not frozen to the bed).

455 For this estimate we have taken this as the area with (modern) ice velocities >50 m a^{-1} from the MEaSUREs v2 dataset, 2017-2018 velocities (Howat, 2017). One outstanding issue with this method of calculating glacial erosion rates is the potential storage of glacially-derived material elsewhere in the system (cf. Cowton et al., 2012; Fernandez et al., 2016). Based on cores recovered from beneath the floating Petermann Ice Tongue (Reilly et al., *In press*) there is at least some unconsolidated sediment cover beneath the tongue, and the modelled bathymetry there (based on a gravity inversion) also indicates the

460 presence of an inner basin and sill with "some non-magnetic sediment cover" (Tinto et al., 2015). This inner basin may hold a considerable volume of ice-proximal sediment deposited since the grounding line has been close to its present location in the fjord. Assuming, for example, 30 m of sediment fill across the basin (approximately 10 x 20 km in size after Tinto et al., 2015) adds 14 km^3 of glacigenic sediment to the total volume and increases the estimated average erosion rate to 0.39-0.45 mm a^{-1}. Additional material may also be stored subglacially upstream of the grounding line and recent studies from Greenland confirm

465 that tens of meters of sediment is indeed present in places (Walter et al., 2014). However, previous studies of glaciomarine sediment volumes from a range of Northern and Southern hemisphere fjords assume that the change in storage is negligible compared to the volume of material delivered to the fjord, particularly over 10^2-10^3 year timescales (Hallet et al., 1996; Koppes and Hallet, 2002; Fernandez et al., 2016) and we rely on the same assumption here. Nevertheless, for this reason and because we cannot quantify the amount of sediment that exits the system in icebergs, our estimate should be taken as a *minimum* glacial

470 erosion rate for the Petermann system.

Erosion rates (and sediment fluxes) are likely to vary during a glacial-deglacial cycle because of both pulsed ice streaming (e.g., Christoffersen et al., 2010) and because early in the deglacial period ice streaming may have been over unconsolidated sediment recently deposited during the preceding glacial advance (Elverhøi et al., 1998). Furthermore, increased erosion rates have been correlated with higher ice velocities associated with recent glacial retreat (Koppes and Hallet, 2002, 2006; Koppes

475 et al., 2009). Because of the physiography of the Petermann Fjord system, we are able distinguish between an "earlier" deglacial sediment volume (Petermann GZW and Hall Basin units), when the grounding line was on the fjord-mouth sill and deposition was only on the sill and in Hall Basin, from a "later" deglacial sediment volume (Petermann Fjord units) when grounded ice was retreating through the fjord. Using chronologies from Jakobsson et al. (2018), we can estimate an erosion rate for these two phases of deglaciation. Calculated $\bar{E}$ for 8.7-7.6 ka when the Petermann Ice Stream was at the fjord mouth

480 is 1.41-1.85 mm a^{-1}. For the later phase, recent core chronologies show that the fjord was covered by a floating ice tongue by 6.9 ka (Reilly et al., *In press*), and therefore must have been free from grounded ice by that time. This implies grounding-line retreat through the fjord in as little as 700 years. Assuming again that all but the upper 0.5 m of fjord infill was deposited during this retreat returns a second-phase deglacial $\bar{E}$ (7.6 ka to present) of 0.14 mm a^{-1}. These two values indicate that deglacial erosion rates may have been an order of magnitude larger during the early deglacial when Petermann Ice Stream was grounded

485 on the sill. Presumably, at this time, ice was thinning and warmer basal temperatures led to enhanced ice flow at the bed (cf.

Koppes and Montgomery, 2009) and the ice stream was also in an expanded state allowing for relatively high erosion rates. Furthermore, there is landform evidence that surface meltwater may have reached the bed at this time (Jakobsson et al., 2018) thereby increasing the potential for subglacial erosion. We have to acknowledge that some sediment in inner Hall Basin may have been produced by ice in Kennedy Channel, rather than the Petermann Ice Stream, which would artificially raise the early

490   phase erosion rate calculated here. It is not possible to separate these two components based on currently available information, meaning the early phase erosion rate may be overestimated. However, our results are in line with past work showing that glacial erosion rates vary significantly over different timescales (cf. Koppes and Montgomery, 2009) and with different glaciologic states particularly during retreat when the glacier system experiences rapid changes (e.g., Hallet et al., 1996; Koppes and Hallet, 2002, 2006).

6.3 Comparisons with other fjord systems

There are relatively few previous studies that derive glacial sediment volumes, fluxes or basin-scale erosion rates for Greenland, and none (for erosion rates) that we are aware of that use volumetric analyses in fjords. Thus, it remains difficult to directly compare our results with other systems although recent mapping campaigns in the palaeo-catchment area of the NEGIS ice stream in North-East Greenland (Roberts et al., 2017) will allow for a similar detailed study of that system. One

500   possibly unusual feature of the Petermann Fjord-Nares Strait system is the absence of any thick (several hundreds of metres) accumulations of ice-proximal sediments beyond the fjord-mouth sill, particularly when the ice margin is known to have stabilised there for a period during retreat. As an analogue, a basin in front of the Jakobshavn Isfjord fjord-mouth sill holds more than 250 m of ice-proximal material deposited when the ice margin was at the sill (Hogan et al., 2012; Streuff et al., 2017) during the Fjord Stade c. 10.6-9.4 ka (Young et al., 2013; Streuff et al., 2017). Similarly, fjords in Norway, East

505   Greenland and Patagonia are known to contain 150-500 m of deglacial infill (Aarseth, 1997; Andrews et al., 1994; Fernandez et al., 2016) and seismic profiles of the inner shelf basin at the modern Pine Island Glacier ice shelf edge reveal that it holds >300 m of presumed ice-proximal sediment (Gohl, 2010; Nitsche et al., 2013). Given the similarity in fluxes between the palaeo Jakobshavn and Petermann ice streams, we suggest that lack of thick basin fill at Petermann is due to either a shorter period of stabilization there or increased trapping efficiency of the large basin in front of the Jakobshavn sill when compared

510   to the seafloor morphology of Hall Basin, or some combination of both factors.

Considering glacial erosion rates, there are relatively few examples from Greenland. For the Kangerdlugssuaq Fjord and Trough system in East Greenland, Cowton et al. (2012) updated the modern erosion rate of Andrews et al. (1994) from 0.01 mm a^{-1} to 0.3 mm a^{-1}. The former was based on estimated sediment discharges (for a certain ice flux) and Cowton et al. (2012) included the sediment deposited beneath the mélange (after Syvitski et al., 1996). However, as Cowton et al. noted, the

515   Andrews et al. (1994) study assumed that glacial erosion occurred over the entire Kangerdlugssuaq catchment area (~50 000 km^2) including a large part of the ice-sheet interior which has very low velocities (cf. Rignot and Kanagaratnam, 2006; Howat, 2017). Rather than including portions of the ice sheet interior that are likely frozen to the bed in our glacial catchment in order to compare glacial erosion rates, we elect to decrease the catchment area for Kangerdlugssuaq to areas with ice velocities that

would permit subglacial erosion. Using a catchment area (9437 km^2), which includes only ice flowing at >50 m a^{-1} for the
520   Kangerdlugssuaq system, as we have applied at Petermann, the modern erosion rate for that system becomes 1.46 mm a^{-1}. This
rate is about three times larger than the average deglacial rate for the Petermann system. A useful exercise may be to calculate
the basin-wide deglacial erosion rate for the Jakobshavn catchment area using the volume of glaciomarine sediments deposited
in front of the fjord-mouth sill (29.2 km^3) during an 800 year stillstand (Hogan et al., 2012) and a glacial catchment area
derived using the same procedures in this study (33 504 km^2). This returns a glacial erosion rate for the palaeo-Jakobshavn
525   Isbrae of 0.52 mm a^{-1} and can be compared with the early deglacial erosion rate for Petermann (1.41-1.85 mm a^{-1}), as this was
also calculated for the time when the grounding-line was stable at its fjord mouth. As both systems were drained by a single,
large, fast-flowing ice stream during the last glacial, the lower values for the palaeo-Jakobshavn ice stream may simply reflect
the larger drainage basin used in those calculations (Supp. Fig. 2). We note that the area of fastest-ice flow (>400 m a^{-1}) is
considerably larger in the Petermann system than the Jakobshavn system (Petermann Fjord is about twice as wide) and that
530   rates of glacial erosion are up to four times higher in fjords compared with interfjord areas (Stroeven et al., 2002; Briner et al.,
2006). If the majority of glacial erosion occurs only in these narrow corridors for major outlet glacier systems, then the
calculated glacial erosion rates would differ significantly as the narrow geometry of Jakobshavn would produce a much higher
erosion rate. This indicates the need for a careful and consistent approach to defining the effective drainage basin area in glacial
erosion studies for major outlet glaciers.

535   Modern glacial erosion rates have also been provided for the well-studied Kangerlussuaq area in central West Greenland,
by measuring annual sediment loads (suspended and in solution) in proglacial rivers beyond land-terminating glaciers (Cowton
et al., 2012; Hawkings et al., 2015; Hasholt et al., 2018) and dividing by the catchment area. Although individual study years
have returned rates as high as 4.5 mm a^{-1}, for the decade 2006-2016 the average rate was 0.5 mm a^{-1} (Hasholt et al., 2018).
These studies used a consistent approach to defining the catchment area based on the ablation area for the Kangerlussuaq
540   drainage basin and modelled hydrological catchment, which we deem as comparable to the approach taken here (i.e., they did
not include parts of the ice-sheet interior where erosion is limited). The average modern erosion rate from Kangerlussuaq (0.5
mm a^{-1}) is similar to our average deglacial erosion rate for Petermann (0.29-0.34 mm a^{-1}) despite the differences in
methodologies employed, timescales studied (millennial vs. annual/decadal) and the glaciologic setting (multiple land-
terminating glaciers vs. one large marine-terminating ice stream). Regarding the latter, significant surface melt occurs at
545   Kangerlussuaq that then migrates to the bed via moulins and entrains sediment as it drains subglacially (Cowton et al., 2012).
In contrast, although supra-glacial lakes are documented on the grounded portion of the modern Petermann Glacier during the
summer, and may drain to the bed (MacDonald et al., 2018), the fast flow is the dominant control on basal sliding (cf. Nick et
al., 2012) and, therefore, presumably on glacial erosion for this catchment. Previous studies have suggested that modern rates
may not be representative of longer-term (millennial) rates because of recent increases in subglacial erosion (and/or sediment
550   evacuation) as glaciers accelerate in today's warming climate (Koppes and Montgomery, 2009). This is certainly true for the
GrIS where surface mass balance has become increasingly negative over the last four decades (Mouginot et al., 2018)
suggesting that modern glacial erosion rates have probably started to rapidly accelerate over the last decade. However, the

rates that we calculate for the Petermann system are for a major phase of deglaciation when the ice stream likely accelerated and subglacial erosion was likely enhanced, and therefore may be comparable to accelerated retreat of today's glaciers. Regardless, we must be cautious when comparing rates that employ different procedures and are determined for very different timescales.

There is a large body of previous work using the volume of glaciomarine sediments in fjords to derive sediment yields and, ultimately, glacial erosion rates during retreat (e.g., Powell, 1991; Hunter, 1994; Stravers and Syvitski, 1991; Hallet et al., 1996; Elverhøi et al., 1995; Koppes and Hallet, 2002; Fernandez et al., 2016). Erosion rates for Alaskan glaciers, where the climate is temperate and tectonic uplift are major contributing factors, are exceptionally high (>10-100 mm a^{-1}; Hallet et al., 1996). The study of Fernandez et al. (2016) reported average millennial erosion rates between 0.02 and 0.83 mm a^{-1} for Patagonian and Antarctic Peninsula fjord systems (since deglaciation) and provides a ready comparison to the results of this study. Their values for the Antarctic Peninsula cluster around 0.1 mm a^{-1}, which is comparable to the average value we derive for the Petermann catchment. They also highlight a decrease in erosion rates with increasing latitude that they attribute to decreasing temperatures and availability of liquid water at the ice-rock interface. The Petermann area, situated at ~81° N, has a polar climate with a mean annual temperature (MAT) of around -11°C (for Thule airbase; www.yr.no) at present; based on reconstruction from ice cores, surface air temperatures were around 1-3°C higher than today during deglaciation (Lecavalier et al., 2017). The only system with a comparable MAT in the Fernandez et al. study is Herbert Sound on the Eastern Antarctic Peninsula (MAT = -7.8°C; $\bar{E}$ = 0.12 mm a^{-1}); however, as noted earlier, relatively little surface meltwater accesses the bed in this type of glaciologic setting and the fast-flow of feeder glaciers likely dominates glacial erosion. We suggest that the higher deglacial erosion rate at Petermann compared with the Antarctic Peninsula fjords was, therefore, most likely caused by a high trapping efficiency of the Petermann Fjord-Hall Basin setting in conjunction with the erosive potential of a major (~20 km wide; > 1500 m thick) ice stream draining the area during deglaciation.

7 Conclusions

We present the first comprehensive investigation of the glacial-sedimentary infill of a major fjord system in Greenland. The seismic stratigraphy of Petermann Fjord and the adjacent Nares Strait area confirm the episodic retreat of ice streams in the area marked by GZW deposits, followed by the deposition of sediment from meltwater plumes and icebergs. The rugged bedrock topography is a major control on sediment distribution in relation to the retreating ice margin; redeposition by gravity flows was only important locally. Our mapped unconsolidated sediment volumes provide glacial sediment fluxes for the former Petermann Ice Stream when it was stable on a sill at the fjord mouth that are in line with sediment flux estimates from modern Antarctic and other Northern Hemisphere palaeo-ice streams including the palaeo-Jakobshavn Isbrae. The average deglacial erosion rate that we calculate for the Petermann drainage basin is one of only a few erosion rate estimates for Greenland and is similar to the rates from the Antarctic Peninsula and some Patagonian catchments despite being subject to a much colder climate. In this setting, ice dynamics rather than climate, namely the fast-flow of Petermann Glacier (or former ice stream), is

585   the dominant control on glacial erosion. The order-of-magnitude difference between glacial erosion rates during an early phase of deglaciation (when the grounding line was stable at the fjord mouth) and a later phase (of retreat through the fjord) confirm significant variability in erosion rates related to deglacial retreat rates and ice dynamics. Mapped pre-LGM surfaces, calculated glacial sediment fluxes and our range of glacial erosion rates provide much needed observational constraints on future numerical modelling experiments of the Petermann system, one of the best studied outlet glacier systems in Greenland.

590   **References**

Aarseth, I.: Western Norwegian fjord sediments: age, volume, stratigraphy, and role as temporary depository during glacial cycles, Marine Geology, 143, 39-53, 1997.

Åkesson, H., Nisancioglu, K. H., and Nick, F. M.: Impact of Fjord Geometry on Grounding Line Stability, 6, 2018.

Alley, R. B., Anandakrishnan, S., Dupont, T. K., Parizek, B. R., and Pollard, D.: Effect of Sedimentation on Ice-Sheet
595   Grounding-Line Stability, 315, 1838-1841, 2007.

Amundson, J. M., M. Fahnestock, M. Truffer, J. Brown, M. P. Lüthi, and R. J. Motyka: Ice mélange dynamics and implications for terminus stability, Jakobshavn Isbræ, Greenland, Journal of Geophysical Research, 115, doi:10.1029/2009JF001405, 2010.

Anandakrishnan, S., Catania, G. A., Alley, R. B., and Horgan, H. J.: Discovery of Till Deposition at the Grounding Line of
600   Whillans Ice Stream, Science, 315, 1835-1838, 2007.

Anderson, J. B.: Antarctic Marine Geology, Cambridge University Press, London, 1999.

Andresen, C. S., Straneo, F., Ribergaard, M. H., Bjørk, A. A., Andersen, T. J., Kuijpers, A., Nørgaard-Pedersen, N., Kjær, K. H., Schjøth, F., Weckström, K., and Ahlstrøm, A. P.: Rapid response of Helheim Glacier in Greenland to climate variability over the past century, Nature Geoscience, 5, 37, 2011.

605   Andrews, J. T., Milliman, J. D., Jennings, A. E., Rynes, N., and Dwyer, J.: Sediment Thicknesses and Holocene Glacial Marine Sedimentation Rates in Three East Greenland Fjords (ca. 68°N), The Journal of Geology, 102, 669-683, 1994.

Bjarnadóttir, L. R., Rüther, D. C., Winsborrow, M. C. M., and Andreassen, K.: Grounding-line dynamics during the last deglaciation of Kveithola, W Barents Sea, as revealed by seabed geomorphology and shallow seismic stratigraphy, Boreas, 42, 84-107, 2013.

610   Briner, J. P., Miller, G. H., Davis, P. T., and Finkel, R. C.: Cosmogenic radionuclides from fiord landscapes support differential erosion by overriding ice sheets, GSA Bulletin, 118, 406-420, 2006.

Catania, G. A., Stearns, L. A., Sutherland, D. A., Fried, M. J., Bartholomaus, T. C., Morlighem, M., Shroyer, E., and Nash, J.: Geometric Controls on Tidewater Glacier Retreat in Central Western Greenland, 123, 2024-2038, 2018.

Christoffersen, P., Tulaczyk, S., and Behar, A.: Basal ice sequences in Antarctic ice stream: Exposure of past hydrologic
615   conditions and a principal mode of sediment transfer, Journal of Geophysical Research: Earth Surface, 115, 2010.

Cochrane, G. R., De Santis, L., and Cooper, A. K.: Seismic velocity expression of glacial sedimentary rocks beneath the Ross Sea from sonobuoy seismic-refraction data, Antarctic Research Series, 68, 261-270, 1995.

Cowan, E. A., Seramur, K. C., Powell, R. D., Willems, B. A., Gulick, S. P. S., and Jaeger, J. M.: Fjords as temporary sediment traps: History of glacial erosion and deposition in Muir Inlet, Glacier Bay National Park, southeastern Alaska, GSA
620   Bulletin, 122, 1067-1080, 2010.

Cowton, T., Nienow, P., Bartholomew, I., Sole, A., and Mair, D.: Rapid erosion beneath the Greenland ice sheet, Geology, 40, 343-346, 2012.

Dawes, W.: Explanatory notes to the Geological map of Greenland, 1:500 000, Humboldt Gletscher, Sheet 6. 1-48, Geological Survey of Denmark and Greenland, Copenhagen, 2004.

625   Desloges, J., Gilbert, R, Nielsen, N, Christiansen, C, Rasch, M, Ohlenschlager, R.: Holocene glaciomarine sedimentary environments in fiords of Disko Bugt, West Greenland., Quaternary Science Reviews, 21, 947-963, 2002.

Dietrich, P., Ghienne, J.-F., Lajeunesse, P., Normandeau, A., Deschamps, R., and Razin, P.: Deglacial sequences and glacio-isostatic adjustment: Quaternary compared with Ordovician glaciations, Geological Society, London, Special Publications, 475, SP475.479, 2018.

630   DMI: https://www.dmi.dk/en/groenland/hav/ice-charts/, 2018.

Dowdeswell, J. and Fugelli, E.: The seismic architecture and geometry of grounding-zone wedges formed at the marine margins of past ice sheets, Geological Society of America Bulletin, 124, 1750-1761, 2012.

Dowdeswell, J., Whittington, R., Jennings, A., Andrews, J., Mackensen, A., and Marienfeld, P.: An origin for laminated glaciomarine sediments through sea-ice build-up and suppressed iceberg rafting, Sedimentology, 47, 557-576, 2000.

635   Dowdeswell, J. A., Canals, M., Jakobsson, M., Todd, B. J., Dowdeswell, E. K., and Hogan, K. A.: Introduction: an Atlas of Submarine Glacial Landforms, Geological Society, London, Memoirs, 46, 3-14, 2016.

Dowdeswell, J. A., Ó Cofaigh, C., Taylor, J., Kenyon, N. H., Mienert, J., and Wilken, M.: On the architecture of high-latitude continental margins: the influence of ice-sheet and sea-ice processes in the Polar North Atlantic, Geological Society, London, Special Publications, 203, 33, 2002.

640   Dowdeswell, J. A. and Ottesen, D.: Buried iceberg ploughmarks in the early Quaternary sediments of the central North Sea: A two-million year record of glacial influence from 3D seismic data, Marine Geology, 344, 1-9, 2013.

Dowdeswell, J. A., Whittington, R. J., and Marienfeld, P.: The origin of massive diamicton facies by iceberg rafting and scouring, Scoresby Sund, East Greenland, Sedimentology, 41, 21-35, 1994.

Dühnforth, M., Anderson, R. S., Ward, D., and Stock, G. M.: Bedrock fracture control of glacial erosion processes and rates,
645   Geology, 38, 423-426, 2010.

Elverhøi, A., Hooke, R. L., and Solheim, A.: Late Cenozoic erosion and sediment yield from the Svalbard–Barents Sea region: implications for understanding erosion of glacierized basins, Quaternary Science Reviews, 17, 209-241, 1998.

Elverhøi, A., Svendsen, J. I., Solheim, A., Andersen, E. S., Milliman, J., Mangerud, J., and Hooke, R. L.: Late Quaternary Sediment Yield from the High Arctic Svalbard Area, The Journal of Geology, 103, 1-17, 1995.

The Cryosphere
Discussions

650 Enderlin, E. M., Howat, I. M., Jeong, S., Noh, M.-J., van Angelen, J. H., and van den Broeke, M. R.: An improved mass budget for the Greenland ice sheet, Geophysical Research Letters, 41, 866-872, 2014.

Engelhardt, H. F. and Kamb, B.: Basal sliding of Ice Stream B, West Antarctica, Journal of Glaciology, 44, 223-230, 1998.

England, J.: Coalescent Greenland and Innuitian ice during the Last Glacial Maximum: revising the Quaternary of the Canadian High Arctic, Quaternary Science Reviews, 18, 421-456, 1999.

655 England, J., Atkinson, N., Bednarski, J., Dyke, A. S., Hodgson, D. A., and Ó Cofaigh, C.: The Innuitian Ice Sheet: configuration, dynamics and chronology, Quaternary Science Reviews, 25, 689-703, 2006.

Esteves, M., Bjarnadóttir, L. R., Winsborrow, M. C. M., Shackleton, C. S., and Andreassen, K.: Retreat patterns and dynamics of the Sentralbankrenna glacial system, central Barents Sea, Quaternary Science Reviews, 169, 131-147, 2017.

Eyles, N.: Earth's glacial record and its tectonic setting, Earth-Science Reviews, 35, 1-248, 1993.

660 Fernandez, R. A., Anderson, J. B., Wellner, J. S., Minzoni, R. L., Hallet, B., and Smith, R. T.: Latitudinal variation in glacial erosion rates from Patagonia and the Antarctic Peninsula (46°S–65°S), GSA Bulletin, 128, 1000-1023, 2016.

Flink, A. E., Noormets, R., Kirchner, N., Benn, D. I., Luckman, A., and Lovell, H.: The evolution of a submarine landform record following recent and multiple surges of Tunabreen glacier, Svalbard, Quaternary Science Reviews, 108, 37-50, 2015.

665 Forwick, M., Vorren, T. O., Hald, M., Korsun, S., Roh, Y., Vogt, C., and Yoo, K.-C.: Spatial and temporal influence of glaciers and rivers on the sedimentary environment in Sassenfjorden and Tempelfjorden, Spitsbergen, 344, 163-193, 2010.

Funder, S., Kjeldsen, K. K., Kjær, K. H., and Ó Cofaigh, C.: Chapter 50 - The Greenland Ice Sheet During the Past 300,000 Years: A Review. In: Developments in Quaternary Sciences, Ehlers, J., Gibbard, P. L., and Hughes, P. D. (Eds.), Elsevier, 2011.

670 Georgiadis, E., Giraudeau, J., Martinez, P., Lajeunesse, P., St-Onge, G., Schmidt, S., and Massé, G.: Deglacial to postglacial history of Nares Strait, Northwest Greenland: a marine perspective from Kane Basin, Clim. Past, 14, 1991-2010, 2018.

Gilbert, R., Nielsen, N, Möller, H, Desloges, JR, Rasch, M.: Glaciomarine sedimentation in Kangerdluk (Disko Fjord), West Greenland, in response to a surging glacier. , Marine Geology, 191, 1-18, 2002.

675 Gilbert, R., Aitken, A. E., and Lemmen, D. S.: The glaciomarine sedimentary environment of Expedition Fiord, Canadian High Arctic, Marine Geology, 110, 257-273, 1993.

Gilbert, R., Nielsen, N., Desloges, J. R., and Rasch, M.: Contrasting glaciomarine sedimentary environments of two arctic fiords on Disko, West Greenland, Marine Geology, 147, 63-83, 1998.

Gohl, K.: Basement control on past ice sheet dynamics in the Amundsen Sea Embayment, West Antarctica, Palaeogeography,
680 Palaeoclimatology, Palaeoecology, 335-336, 35-41, 2012.

Golledge, N. R., Levy, R. H., McKay, R. M., Fogwill, C. J., White, D. A., Graham, A. G. C., Smith, J. A., Hillenbrand, C.-D., Licht, K. J., Denton, G. H., Ackert, R. P., Maas, S. M., and Hall, B. L.: Glaciology and geological signature of the Last Glacial Maximum Antarctic ice sheet, Quaternary Science Reviews, 78, 225-247, 2013.

Goudie, A. S.: The Schmidt Hammer in geomorphological research, Progress in Physical Geography: Earth and Environment, 30, 703-718, 2006.

Hallet, B., Hunter, L., and Bogen, J.: Rates of erosion and sediment evacuation by glaciers: A review of field data and their implications, Global and Planetary Change, 12, 213-235, 1996.

Hasholt, B., van As, D., Mikkelsen, A. B., Mernild, S. H., and Yde, J. C.: Observed sediment and solute transport from the Kangerlussuaq sector of the Greenland Ice Sheet (2006–2016), Arctic, Antarctic, and Alpine Research, 50, S100009, 2018.

Hawkings, J. R., Wadham, J. L., Tranter, M., Lawson, E., Sole, A., Cowton, T., Tedstone, A. J., Bartholomew, I., Nienow, P., Chandler, D., and Telling, J.: The effect of warming climate on nutrient and solute export from the Greenland Ice Sheet, Geochemical Perspectives Letters, 1, 94-104, 2015.

Henriksen, N., Higgins, A. K., Kalsbeek, F., and Pulvertaft, T. C.: Greenland from Archaean to Quaternary Descriptive text to the 1995 Geological map of Greenland, 1:2 500 000., Geological Survey of Denmark and Greenland Bulletin, 18, 126, 2009.

Hesse, R., Khodabakhsh, S., Klaucke, I., and Ryan, W. B. F.: Asymmetrical turbid surface-plume deposition near ice-outlets of the Pleistocene Laurentide ice sheet in the Labrador Sea, Geo-Marine Letters, 17, 179-187, 1997.

Heuzé, C., Wåhlin, A., Johnson, H. L., and Münchow, A.: Pathways of Meltwater Export from Petermann Glacier, Greenland, Journal of Physical Oceanography, 47, 405-418, 2016.

Hill, E. A., Carr, J. R., Stokes, C. R., and Gudmundsson, G. H.: Dynamic changes in outlet glaciers in northern Greenland from 1948 to 2015, The Cryosphere, 12, 3243-3263, 2018.

Hjelstuen, B. O., Haflidason, H., Sejrup, H. P., and Lyså, A.: Sedimentary processes and depositional environments in glaciated fjord systems — Evidence from Nordfjord, Norway, Marine Geology, 258, 88-99, 2009.

Hofstede, C., Christoffersen, P., Hubbard, B., Doyle, S. H., Young, T. J., Diez, A., Eisen, O., and Hubbard, A.: Physical Conditions of Fast Glacier Flow: 2. Variable Extent of Anisotropic Ice and Soft Basal Sediment From Seismic Reflection Data Acquired on Store Glacier, West Greenland, Journal of Geophysical Research: Earth Surface, 123, 349-362, 2018.

Hogan, K., Dowdeswell, J., and Cofaigh, C. Ó.: Glaciomarine sedimentary processes and depositional environments in an embayment fed by West Greenland ice streams, Marine Geology, 311, 1-16, 2012.

Hogan, K. A., Dix, J. K., Lloyd, J. M., Long, A. J., and Cotterill, C. J.: Seismic stratigraphy records the deglacial history of Jakobshavn Isbræ, West Greenland, Journal of Quaternary Science, 26, 757, 2011.

Holland, D. M., Thomas, R. H., De Yound, B., Ribergaard, M. H., and Lyberth, B.: Acceleration of Jakobshavn Isbrae triggered by warm subsurface ocean waters, Nature Geoscience, 1, 659-664, 2008.

Hooke, R. and Elverhøi, A.: Sediment flux from a fjord during glacial periods, Isfjorden, Spitsbergen, Global and Planetary Change, 12, 237-249, 1996.

Howat, I. M.: MEaSUREs Greenland Ice Velocity: Selected Glacier Site Velocity Maps from Optical Images, Version 2.
Howat, I. M. (Ed.), NASA National Snow and Ice Data Center Distributed Active Archive Center. Ice Veolcity.,
Boulder, Colorado USA, 2017.

720 Howe, J. A., Austin, W. E. N., Forwick, M., Paetzel, M., Harland, R., and Cage, A. G.: Fjord systems and archives: a review,
344, 5-15, 2010.

Hunter, L.: Grounding-line systems of modern temperate glaciers and their effects on glacier stability, Ph.D, Northern Illinois
University, De Kalb, 467 pp., 1994.

Jackson, H. R., Hannon, T., Neben, S., Piepjohn, K., and Brent, T.: Seismic Reflection Profiles from Kane to Hall Basin, Nares
725   Strait: Evidence for Faulting, Polarforschung, 74, 21-39, 2006.

Jakobsson, M., Hogan, K. A., Mayer, L. A., Mix, A., Jennings, A., Stoner, J., Eriksson, B., Jerram, K., Mohammad, R., Pearce,
C., Reilly, B., and Stranne, C.: The Holocene retreat dynamics and stability of Petermann Glacier in northwest
Greenland, Nature Communications, 9, 2104, 2018.

Jakobsson, M., Mayer, L., Coakley, B., Dowdeswell, J. A., Forbes, S., Fridman, B., Hodnesdal, H., Noormets, R., Pedersen,
730   R., Rebesco, M., Schenke, H. W., Zarayskaya, Y., Accettella, D., Armstrong, A., Anderson, R. M., Bienhoff, P.,
Camerlenghi, A., Church, I., Edwards, M., Gardner, J. V., Hall, J. K., Hell, B., Hestvik, O., Kristoffersen, Y.,
Marcussen, C., Mohammad, R., Mosher, D., Nghiem, S. V., Pedrosa, M. T., Travaglini, P. G., and Weatherall, P.:
The International Bathymetric Chart of the Arctic Ocean (IBCAO) Version 3.0, Geophysical Research Letters, 39,
2012.

735 Jennings, A., Reilly, B., Andrews, J., Walczak, M., Stoner, J., Mix, A., and Jakobsson, M.: Sediment and Faunal Evidence of
Ice Shelves and Their Disintegration during the Early Holocene Deglaciation of Nares Strait, 2018.

Jennings, A. E., Andrews, J. T., Oliver, B., Walczak, M., and Mix, A.: Retreat of the Smith Sound Ice Stream in the Early
Holocene, Boreas, 0, 2019.

Jennings, A. E., Sheldon, C., Cronin, T. M., Francus, P., Stoner, J., and Andrews, J.: THE HOLOCENE HISTORY OF NARES
740   STRAIT: Transition from Glacial Bay to Arctic-Atlantic Throughflow, Oceanography, 24, 26-41, 2011.

Jennings, A. E. and Weiner, N. J.: Environmental change in eastern Greenland during the last 1300 years: evidence from
foraminifera and lithofacies in Nansen Fjord, 68 N, The Holocene, 6, 179-191, 1996.

Johnson, H. L., Münchow, A., Falkner, K. K., and Melling, H.: Ocean circulation and properties in Petermann Fjord,
Greenland, Journal of Geophysical Research: Oceans, 116, 2011.

745 K., L.-M., Jakobsson, M., Mix, A., Freire, F., Hogan, K., Mayer, L., and Smultea, M. A.: Seal occurrence and habitat use
during summer in Petermann Fjord, northwestern Greenland, Arctic, 71, 334-349, 2018.

Kamb, B.: Basal Zone of the West Antarctic Ice Streams and its Role in Lubrication of Their Rapid Motion. In: The West
Antarctic Ice Sheet: Behavior and Environment, Antarctic Research Series, Antarctic Research Series, 2001.

King, E. C., Woodward, J., and Smith, A. M.: Seismic and radar observations of subglacial bed forms beneath the onset zone
750   of Rutford Ice Stream, Antarctica, Journal of Glaciology, 53, 665-672, 2007.

King, E. C., Woodward, J., and Smith, A. M.: Seismic evidence for a water-filled canal in deforming till beneath Rutford Ice Stream, West Antarctica, Geophysical Research Letters, 31, 2004.

Koppes, M. and Hallet, B.: Erosion rates during rapid deglaciation in Icy Bay, Alaska, Journal of Geophysical Research: Earth Surface, 111, 2006.

755   Koppes, M., Hallet, B., Rignot, E., Mouginot, J., Wellner, J. S., and Boldt, K.: Observed latitudinal variations in erosion as a function of glacier dynamics, Nature, 526, 100, 2015.

Koppes, M. l. N. and Hallet, B.: Influence of rapid glacial retreat on the rate of erosion by tidewater glaciers, Geology, 30, 47-50, 2002.

Koppes, M. N. and Montgomery, D. R.: The relative efficacy of fluvial and glacial erosion over modern to orogenic timescales, Nature Geoscience, 2, 644, 2009.

760

Krabbendam, M. and Glasser, N. F.: Glacial erosion and bedrock properties in NW Scotland: Abrasion and plucking, hardness and joint spacing, Geomorphology, 130, 374-383, 2011.

Laberg, J. S. and Vorren, T. O.: The Trænadjupet Slide, offshore Norway – morphology, evacuation and triggering mechanisms, Marine Geology, 171, 95-114, 2000.

765   Larsen, N. K., Kjær, K. H., Funder, S., Möller, P., van der Meer, J. J. M., Schomacker, A., Linge, H., and Darby, D. A.: Late Quaternary glaciation history of northernmost Greenland – Evidence of shelf-based ice, Quaternary Science Reviews, 29, 3399-3414, 2010.

Larter, R. D. and Vanneste, L. E.: Relict subglacial deltas on the Antarctic Peninsula outer shelf, Geology, 23, 33-36, 1995.

Lecavalier, B. S., Fisher, D. A., Milne, G. A., Vinther, B. M., Tarasov, L., Huybrechts, P., Lacelle, D., Main, B., Zheng, J.,

770   Bourgeois, J., and Dyke, A. S.: High Arctic Holocene temperature record from the Agassiz ice cap and Greenland ice sheet evolution, Proceedings of the National Academy of Sciences, 114, 5952, 2017.

Madaj, L.: Holocene Organic Carbon and Carbonate Records from Northeast Baffin Bay: Preliminary Age Model and Paleoenvironmental Significance, MSc, Department of Earth Sciences, University of Gothenburg, Gothenburg, 48 pp., 2016.

775   Möller, P., Larsen, N. K., Kjær, K. H., Funder, S., Schomacker, A., Linge, H., and Fabel, D.: Early to middle Holocene valley glaciations on northernmost Greenland, Quaternary Science Reviews, 29, 3379-3398, 2010.

Mouginot, J., Rignot, E., Bjørk, A. A., van den Broeke, M., Millan, R., Morlighem, M., Noël, B., Scheuchl, B., and Wood, M.: Forty-six years of Greenland Ice Sheet mass balance from 1972 to 2018, Proceedings of the National Academy of Sciences, 116, 9239, 2019.

780   Mudie, P. J., Rochon, A., Prins, M. A., Soenarjo, D., Troelstra, S. R., Levac, E., Scott, D. B., Roncaglia, L., and Kuijpers, A.: Late Pleistocene-Holocene Marine Geology of Nares Strait Region: Palaeoceanography from Foraminifera and Dinoflagellate Cysts, Sedimentology and Stable Isotopes, Polarforschung, 74, 169-183, 2006.

Münchow, A., Melling, H., and Falkner, K. K.: An Observational Estimate of Volume and Freshwater Flux Leaving the Arctic Ocean through Nares Strait, Journal of Physical Oceanography, 36, 2025-2041, 2006.

785   Münchow, A., Padman, L., Washam, P., and Nicholls, K. W.: The Ice Shelf Of Petermann Gletscher, North Greenland, And
            Its Connection To The Arctic And Atlantic Oceans, Oceanography, 29, 84-95, 2016.

       Nitsche, F. O., Gohl, K., Larter, R. D., Hillenbrand, C. D., Kuhn, G., Smith, J. A., Jacobs, S., Anderson, J. B., and Jakobsson,
            M.: Paleo ice flow and subglacial meltwater dynamics in Pine Island Bay, West Antarctica, The Cryosphere, 7, 249-
            262, 2013.

790   Nygård, A.: Pleistocene sedimentary processes and glacial history of the Southern Norwegian continental margin, Ph.D,
            University of Bergen, Bergen, 126 pp., 2003.

       Nygård, A., Sejrup, H. P., Haflidason, H., Lekens, W. A. H., Clark, C. D., and Bigg, G. R.: Extreme sediment and ice discharge
            from marine-based ice streams: New evidence from the North Sea, Geology, 35, 395-398, 2007.

       Ó Cofaigh, C., Dowdeswell, J. A., Allen, C. S., Hiemstra, J. F., Pudsey, C. J., Evans, J., and J.A. Evans, D.: Flow dynamics
795   and till genesis associated with a marine-based Antarctic palaeo-ice stream, Quaternary Science Reviews, 24, 709-
            740, 2005.

       Ottesen, D. and Dowdeswell, J. A.: Assemblages of submarine landforms produced by tidewater glaciers in Svalbard, Journal
            of Geophysical Research: Earth Surface, 111, 2006.

       Pollard, D., DeConto, R. M., and Alley, R. B.: Potential Antarctic Ice Sheet retreat driven by hydrofracturing and ice cliff
800   failure, Earth and Planetary Science Letters, 412, 112-121, 2015.

       Powell, R. D.: Glaciomarine processes and inductive lithofacies modelling of ice shelf and tidewater glacier sediments based
            on Quaternary examples, Marine Geology, 57, 1-52, 1984.

       Powell, R. D.: Grounding-line systems as secondorder controls on fluctuations of tidewater termini of temperate glaciers. In:
            Glacial marine sedimentation; paleoclimatic significance, Anderson, J. B. and Ashley, G. M. (Eds.), Geological
805   Society of America Special Paper, Geological Society of America, 1991.

       Powell, R. D.: Subaquatic Landsystems: fjord. In: Glacial Landsystems, Evans, D. J. A. (Ed.), Hodder Arnold, London, 2005.

       Powell, R. D. and Molnia, B. F.: Glaciomarine sedimentary processes, facies and morphology of the south-southeast Alaska
            shelf and fjords, Marine Geology, 85, 359-390, 1989.

       Reilly, B., Stoner, J., Mix, A., Walczak, M. H., Jennings, A., Jakobsson, M., Dyke, L., Glueder, A., Nicholls, K. W., Hogan,
810   K., Mayer, L. A., Hatfield, R., Fallon, S., and Cheseby, M.: Holocene Break-up and Reestablishment of the Petermann
            Ice Tongue, Northwest Greenland, Quaternary Science Reviews, In Press. 1-59, In Press.

       Reimer, P. J., Bard, E., Bayliss, A., Beck, J. W., Blackwell, P. G., Ramsey, C. B., Buck, C. E., Cheng, H., Edwards, R. L.,
            Friedrich, M., Grootes, P. M., Guilderson, T. P., Haflidason, H., Hajdas, I., Hatté, C., Heaton, T. J., Hoffmann, D. L.,
            Hogg, A. G., Hughen, K. A., Kaiser, K. F., Kromer, B., Manning, S. W., Niu, M., Reimer, R. W., Richards, D. A.,
815   Scott, E. M., Southon, J. R., Staff, R. A., Turney, C. S. M., and van der Plicht, J.: IntCal13 and Marine13 Radiocarbon
            Age Calibration Curves 0–50,000 Years cal BP, Radiocarbon, 55, 1869-1887, 2013.

       Rignot, E. and Kanagaratnam, P.: Changes in the Velocity Structure of the Greenland Ice Sheet, Science, 311, 986-990, 2006.

Roberts, D. H., Lloyd, J. M., O Cofaigh, C., Callard, S. L., Grob, H., and Kappelsberger, M.: NEGIS: Understanding the mechanisms controlling the long-term stability of the Northeast Greenland Ice Stream. In: The Expedition PS100 of
820   the Research Vessel POLARSTERN to the Fram Strait in 2016, Kanzow, T. (Ed.), Berichte zur Polar-und Meeresforschung: Reports on Polar and Marine Research, Alfred wegener Institut, Bremerhaven, 2017.

Roberts, D. H. and Long, A. J.: Streamlined bedrock terrain and fast ice flow, Jakobshavns Isbrae, West Greenland: implications for ice stream and ice sheet dynamics, Boreas, 34, 25-42, 2005.

Simkins, L. M., Anderson, J. B., Greenwood, S. L., Gonnermann, H. M., Prothro, L. O., Halberstadt, A. R. W., Stearns, L. A.,
825   Pollard, D., and DeConto, R. M.: Anatomy of a meltwater drainage system beneath the ancestral East Antarctic ice sheet, Nature Geoscience, 10, 691, 2017.

Smith, A. M.: Basal conditions on Rutford Ice Stream, West Antarctica, from seismic observations, Journal of Geophysical Research: Solid Earth, 102, 543-552, 1997.

Smith, W. H. F. and Wessel, P.: Gridding with continuous curvature splines in tension, GEOPHYSICS, 55, 293-305, 1990.

830 Stewart, M. A., Lonergan, L., and Hampson, G.: 3D seismic analysis of buried tunnel valleys in the central North Sea: morphology, cross-cutting generations and glacial history, Quaternary Science Reviews, 72, 1-17, 2013.

Straneo, F., Sutherland, D. A., Holland, D., Gladish, C., Hamilton, G. S., Johnson, H. L., Rignot, E., Xu, Y., and Koppes, M.: Characteristics of ocean waters reaching Greenland's glaciers, Annals of Glaciology, 53, 202-210, 2012.

Stravers, J. A. and Syvitski, J. P. M.: Land-Sea Correlations and Evolution of the Cambridge Fiord Marine Basin during the
835   Last Deglaciation of Northern Baffin Island, Quaternary Research, 35, 72-90, 1991.

Streuff, K., Ó Cofaigh, C., Hogan, K., Jennings, A., Lloyd, J. M., Noormets, R., Nielsen, T., Kuijpers, A., Dowdeswell, J. A., and Weinrebe, W.: Seafloor geomorphology and glaciomarine sedimentation associated with fast-flowing ice sheet outlet glaciers in Disko Bay, West Greenland, Quaternary Science Reviews, 169, 206-230, 2017.

Stroeven, A. P., Fabel, D., Harbor, J., Hättestrand, C., and Kleman, J.: Reconstructing the erosion history of glaciated passive
840   margins: applications of in situ produced cosmogenic nuclide techniques, Geological Society, London, Special Publications, 196, 153, 2002.

Sugden, D. E., Glasser, N., and Clapperton, C. M.: Evolution of Large Roches Moutonnées, Geografiska Annaler: Series A, Physical Geography, 74, 253-264, 1992.

Syvitski, J. P. M., Andrews, J. T., and Dowdeswell, J. A.: Sediment deposition in an iceberg-dominated glaciomarine
845   environment, East Greenland: basin fill implications, Global and Planetary Change, 12, 251-270, 1996.

Syvitski, J. P. M., Burrell, D. C., and Skei, J. M.: Fjords: Processes and Products. Springer-Verlag, New York, 1987.

Tessensohn, F., Jackson, H. R., and Reid, I. D.: The tectonic evolution of Nares strait: implications of new data, Polarforschung, 2006. 191-198, 2006.

Tinto, K. J., Bell, R. E., Cochran, J. R., and Münchow, A.: Bathymetry in Petermann fjord from Operation IceBridge
850   aerogravity, Earth and Planetary Science Letters, 422, 58-66, 2015.

Tulaczyk, S., Kamb, B., Scherer, R. P., and Engelhardt, H. F.: Sedimentary processes at the base of a West Antarctic ice stream; constraints from textural and compositional properties of subglacial debris, Journal of Sedimentary Research, 68, 487-496, 1998.

Walter, F., Chaput, J., and Lüthi, M. P.: Thick sediments beneath Greenland's ablation zone and their potential role in future
855   ice sheet dynamics, Geology, 42, 487-490, 2014.

Warren, C. R. and Hulton, N. R. J.: Topographic and Glaciological Controls on Holocene Ice-Sheet Margin Dynamics. Central West Greenland, Annals of Glaciology, 14, 307-310, 1990.

Witus, A. E., Branecky, C. M., Anderson, J. B., Szczuciński, W., Schroeder, D. M., Blankenship, D. D., and Jakobsson, M.: Meltwater intensive glacial retreat in polar environments and investigation of associated sediments: example from
860   Pine Island Bay, West Antarctica, Quaternary Science Reviews, 85, 99-118, 2014.

Young, N. E., Briner, J. P., Rood, D. H., Finkel, R. C., Corbett, L. B., and Bierman, P. R.: Age of the Fjord Stade moraines in the Disko Bugt region, western Greenland, and the 9.3 and 8.2 ka cooling events, Quaternary Science Reviews, 60, 76-90, 2013.

Data availability

865   The marine geophysical data used in this paper can be obtained by contacting the second author.

Author contributions

K.A.H., M.J. and L.M. conceived the study; they and B.R., A.J., A.M., K.H., E.N., K.J., and C.S. collected the data during the *Petermann 2015 Expedition*. T.N., K.J.A. and E.K. performed some initial mapping. K.A.H. analysed the SBP data, integrated it with the seismic-reflection data and calculated flux and erosion estimates with contributions from M.J., A.J. and B.R. K.A.H.
870   wrote the initial manuscript with substantial contributions from M.J., B.R., A.J. and L.M. All authors contributed to data interpretation and writing of the final manuscript.

Competing interests.

The authors declare no competing interests.

Acknowledgements

885 **Figure 1. Maps of Greenland and the study area. (a) Location of Petermann Glacier and Nares Strait. (b) Location of the study area (red box; Fig. 2) in Petermann Fjord and the adjacent Nares Strait including Hall Basin (HB), Kennedy Channel (KC) and Robeson Channel (RC). Ice flow in marine areas (black arrows) and deglacial ice-sheet margins for the early Holocene (9.3 cal. ka, ~8.7 cal. ka, ~7.6 cal. ka) are also shown for Nares Strait and were compiled from England (1999), Georgiadis et al. (2018), Jakobsson et al. (2018). Dashed lines outside of this area are from Young & Briner (2015) and references therein.**

890

The Cryosphere
Discussions
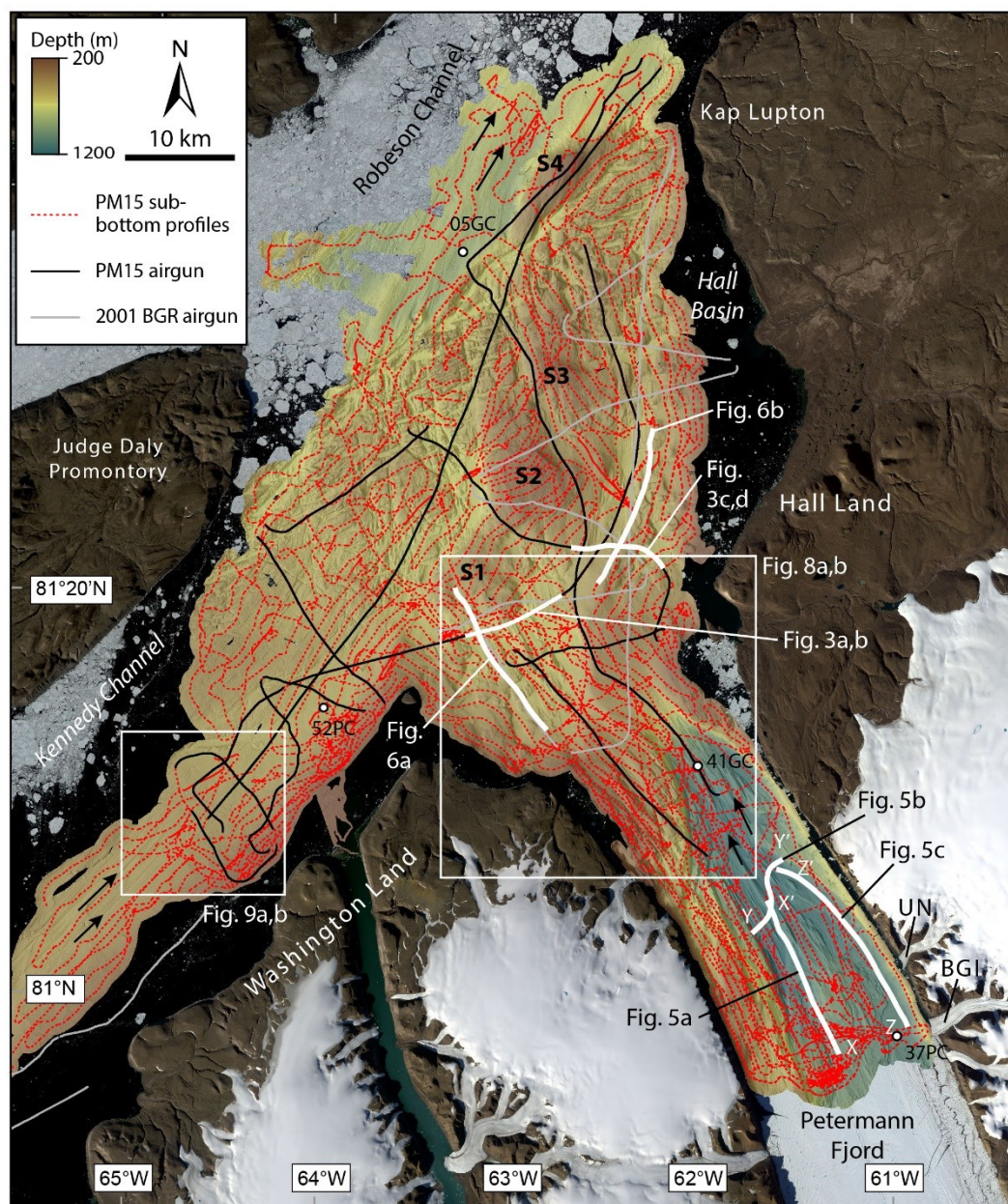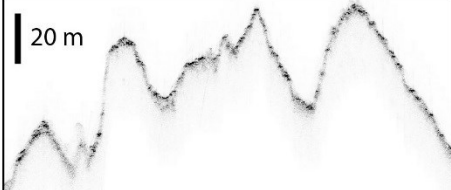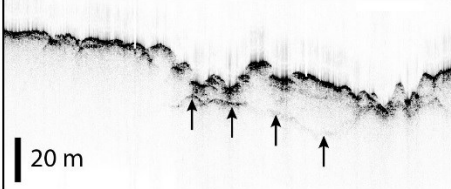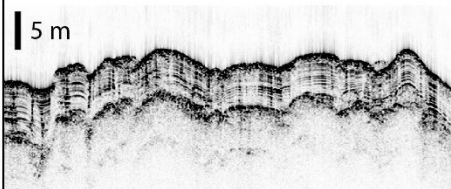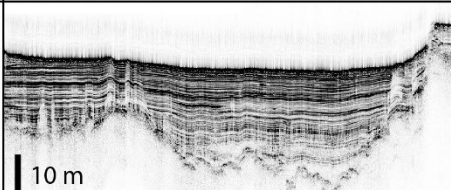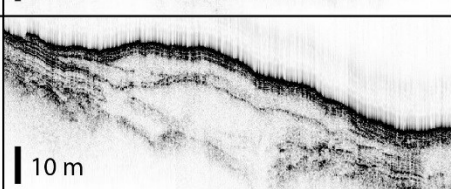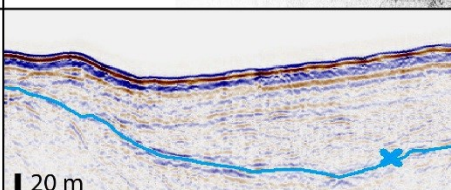
Figure 2: The locations of SBP profiles (red dashed), 2015 AG profiles (black), 2001 legacy AG profiles (grey) shown over the gridded multibeam bathymetry for the area. S1-S4 are the bathymetric highs described by Jakobsson et al. (2018) and referred to in the text. UN is Unnamed Glacier; BGl is Belgrade Glacier. Glacial lineations denoting the former directions of ice flow are shown as black arrows (after Jakobsson et al., 2018). Sediment cores used to correlate seismo-acoustic facies with sediment lithofacies are also shown (see Supplementary Information).
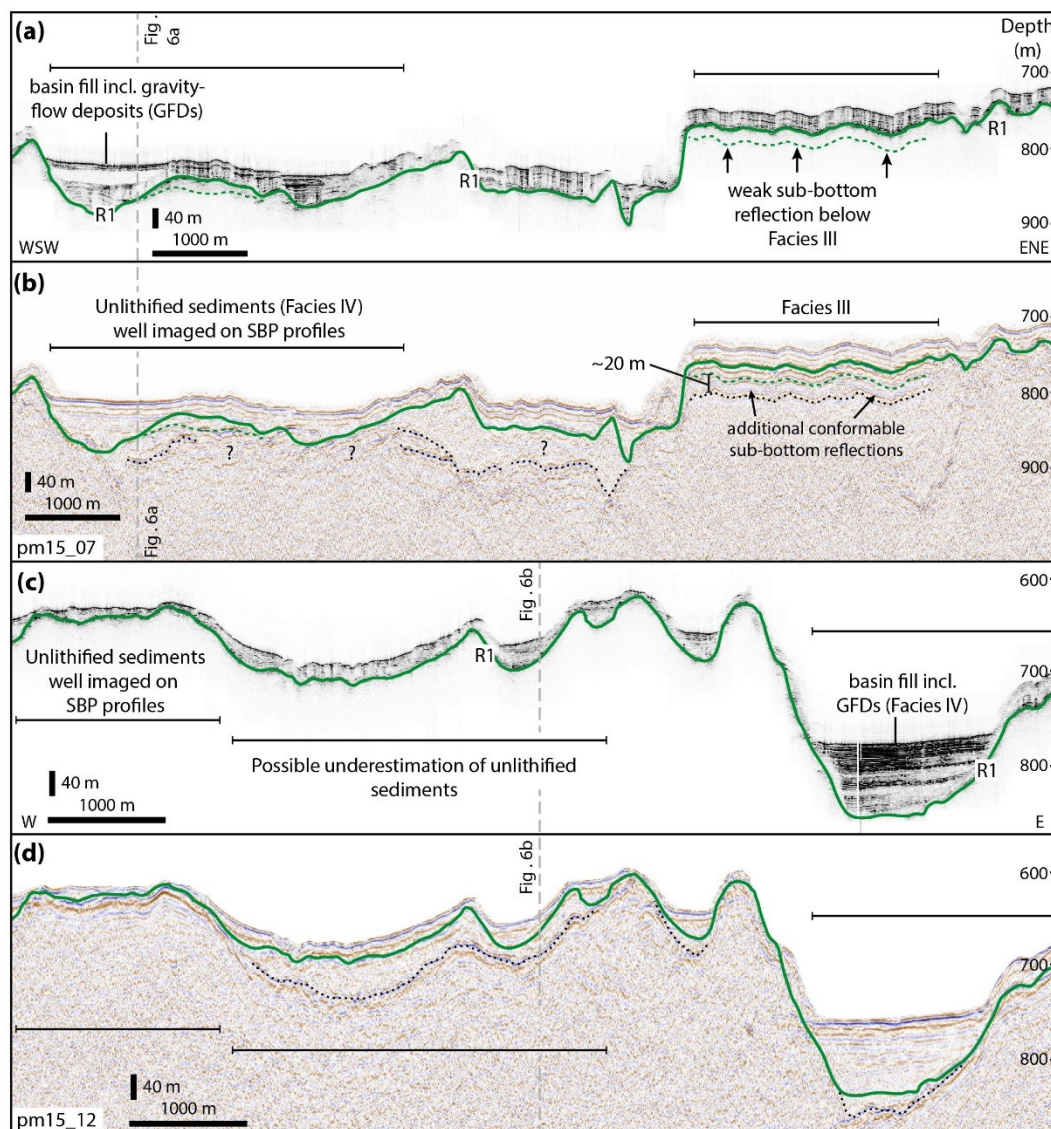
Figure 3. Comparison of SBP profiles with coincident AG profiles showing the mapped basal reflector (R1) on SBP profiles and the corresponding reflector (green) on AG profiles. Dotted lines mark the lowermost reflections on each profile; dotted lines and question marks indicate uncertainty in mapping of unlithified sediment package over basement. Sub-bottom reflections may be geological boundaries in sedimentary bedrock in Hall Basin. (a) SBP profile acquired on 11th August, 2015 in Hall Basin, coincident with AG profile pm15_07 (b). (c) SBP profile from 18th August, 2015 also in Hall Basin, coincident with AG profile pm15_12 (d). Location of profiles is shown in Figure 2; intersection of Fig. 6b with (c) and (d) shown as vertical grey dashed line.

Acoustic facies and configuration	Thickness (m)	Sub-bottom profiler or airgun profile
I. Acoustically-impenetrable to homogenous Moderate to high-amplitude prolonged, continuous reflection defining a rugged surface geometry. Rare sub-bottom point / hyperbolae reflections.	N/A	
II. Acoustically-homogenous to transparent, non-conformable Prolonged upper reflection and discontinuous weak basal reflection. Variable thickness and unconfomable with underlying reflections. Homogenous or transparent.	5 - 20	
III. Acoustically-stratified conformable Medium amplitude, parallel reflections, high continuity, conformable geometry. High-amplitude, continuous upper and basal reflections.	5 - 15	
IV. Acoustically-stratified basin fill Medium amplitude, parallel reflections, high continuity, basin fill (ponded) or onlapping geometry. Occasional thicker transparent units. Continuous upper and basal reflections.	5 - 35	
V. Acoustically-transparent / semi-transparent Low to medium amplitude reflections surrounding acoustically transparent to semi-transparent bodies in basins or on slopes. Geometry is lenticular to variable thickness tapering at one or both ends.	2 - 25 (lenses 2 - 10 m thick)	
VI. Downlapping to chaotic Low amplitude, discontinous reflections with a disorganised downlapping or chaotic geometry. Only observed on AG profiles.	<150	

Figure 4. Seismo-acoustic facies identified from SBP profiles and AG profiles in Petermann Fjord and Nares Strait. Seismo-acoustic facies I-V mapped primarily on SBP profiles and checked with AG profiles; facies VI mapped only from AG profiles.
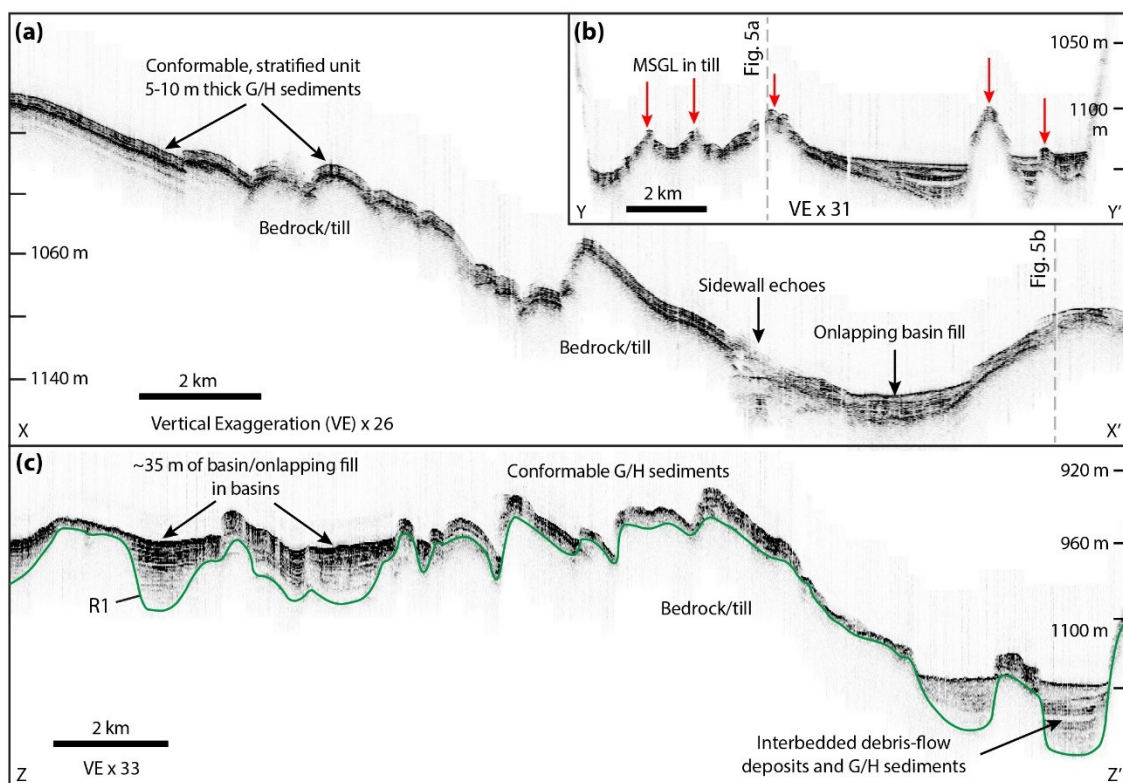
Figure 5. Typical SBP profiles from Petermann Fjord (see Fig. 2 for locations) showing the acoustic stratigraphy of the glaciomarine sediment package. (a) Fjord-parallel line showing conformable units (*Facies III*) overlying R1 reflection. (b) Outer fjord profile running approximately SW-NE showing conformable fill (*Facies III*) over subglacial till deposits (*Facies II*) mapped as MSGL (red arrows) and basin fill with GFDs (*Facies IV*) in local depressions. (c) Fjord-parallel line on the eastern side of the fjord showing basin fill in local depressions and conformable fill elsewhere. G/H is glacimarine/hemipelagic sediments.
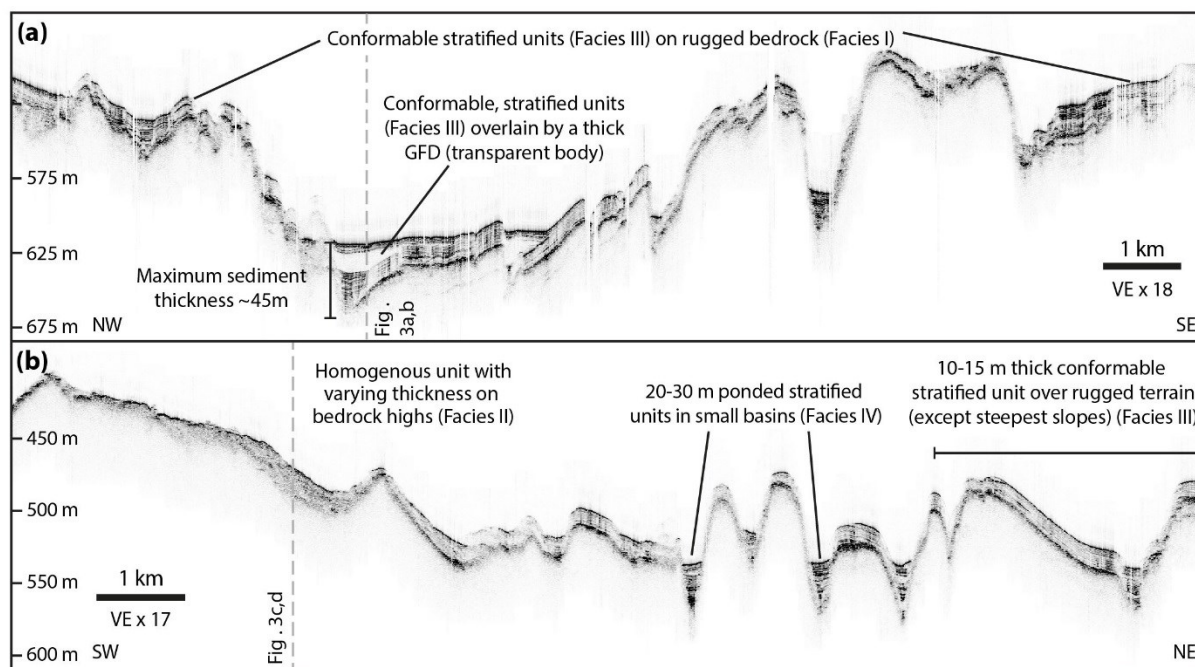
Figure 6. Examples of SBP profiles from Hall Basin, Nares Strait (see Fig. 2 for locations). (a) NW-SE profile in Hall Basin showing bedrock topography (*Facies I*) mantled with conformable sediment (*Facies III*) and ponded basin fill, sometimes with significant GFDs in local depressions (*Facies IV*). (b) A SW-NE profile between the Petermann sill and S1 high showing a similar stratigraphy but including non-conformable, homogenous sediment on steep slopes (*Facies II*). Intersections with Figs. 3a-d are marked with vertical grey dashed lines.
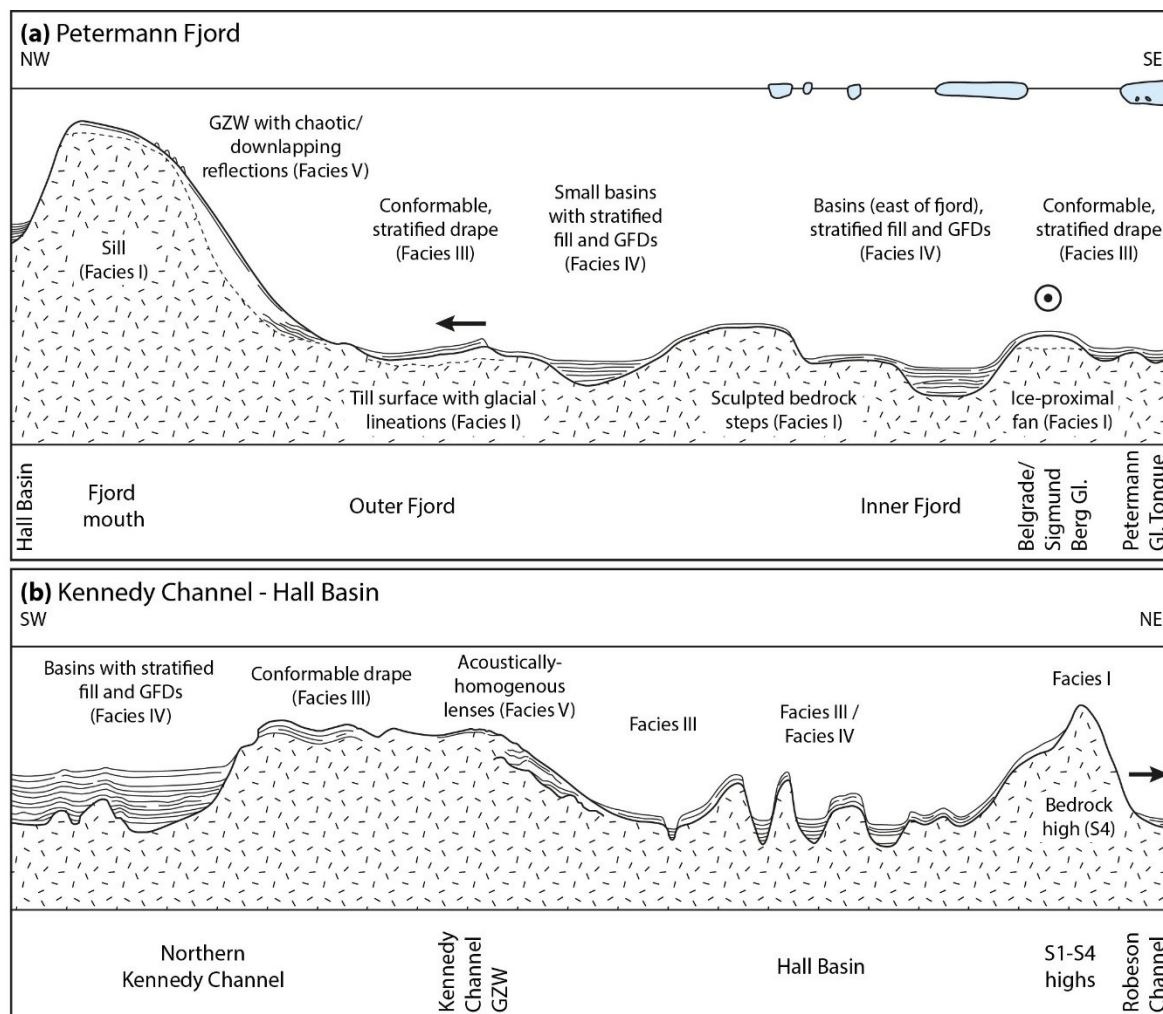
Figure 7. Conceptual transects showing the seismic stratigraphy and distribution of glaciomarine sediments in the Petermann Fjord-Nares Strait area. (a) Petermann Fjord with the fjord-mouth sill with GZW on the left side; localized sediment input into the NE side of the fjord from tributary glaciers and building an ice-proximal fan is shown as the bullseye. (b) Deglacial sediment cover in Nares Strait from Kennedy Channel to Hall Basin to Robeson Channel. Not to scale. Black arrows show the former ice flow direction through the system.
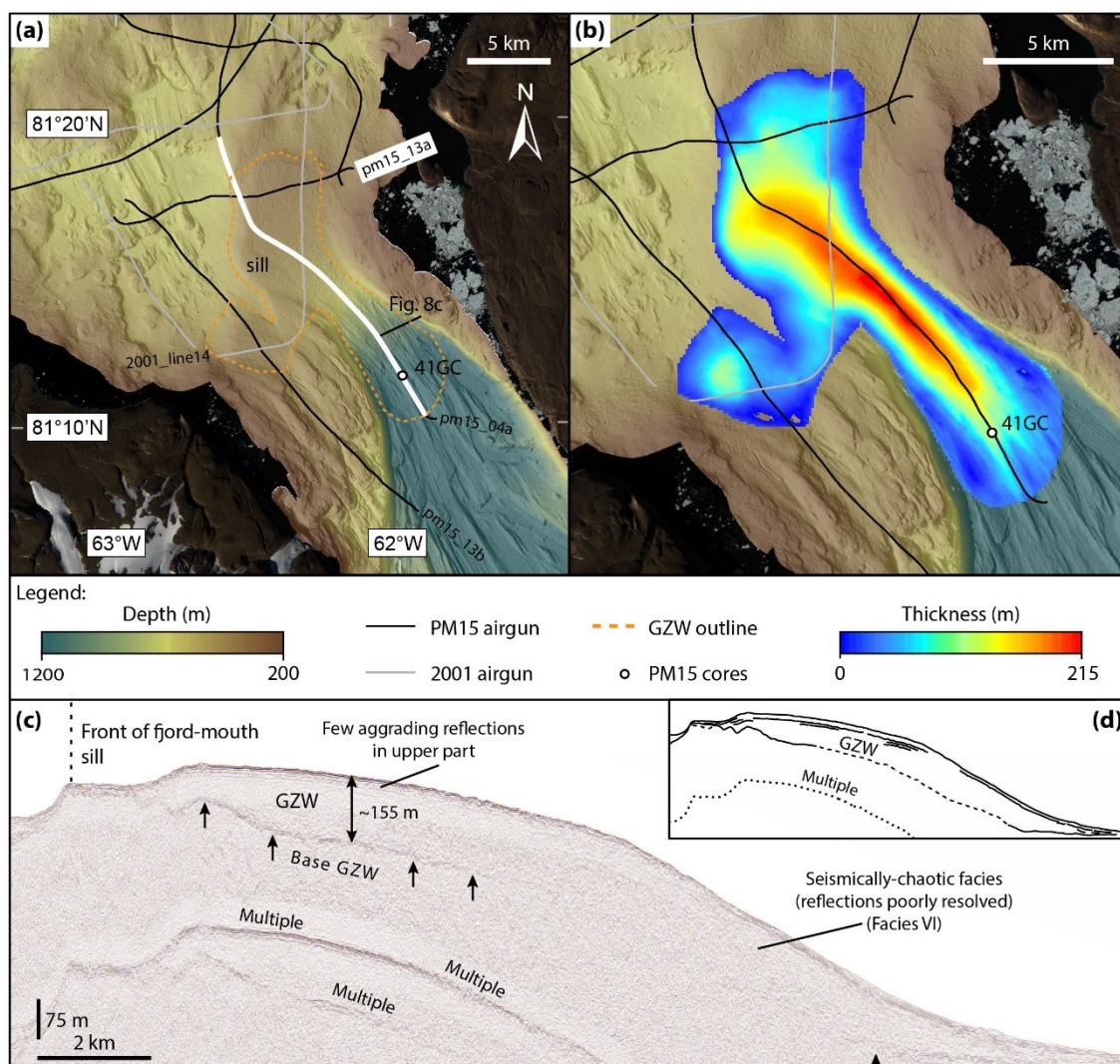
Figure 8. Mapping of the Petermann sill grounding-zone wedge (GZW). (a) AG profiles over the GZW and outline used in volume calculations. (b) Isopach map of the GZW based on mapping from AG lines. (c) AG profile pm15_04a showing the seismic stratigraphy (Facies VI) of the GZW. (d) Line drawing of AG profile pm15_04a.

935
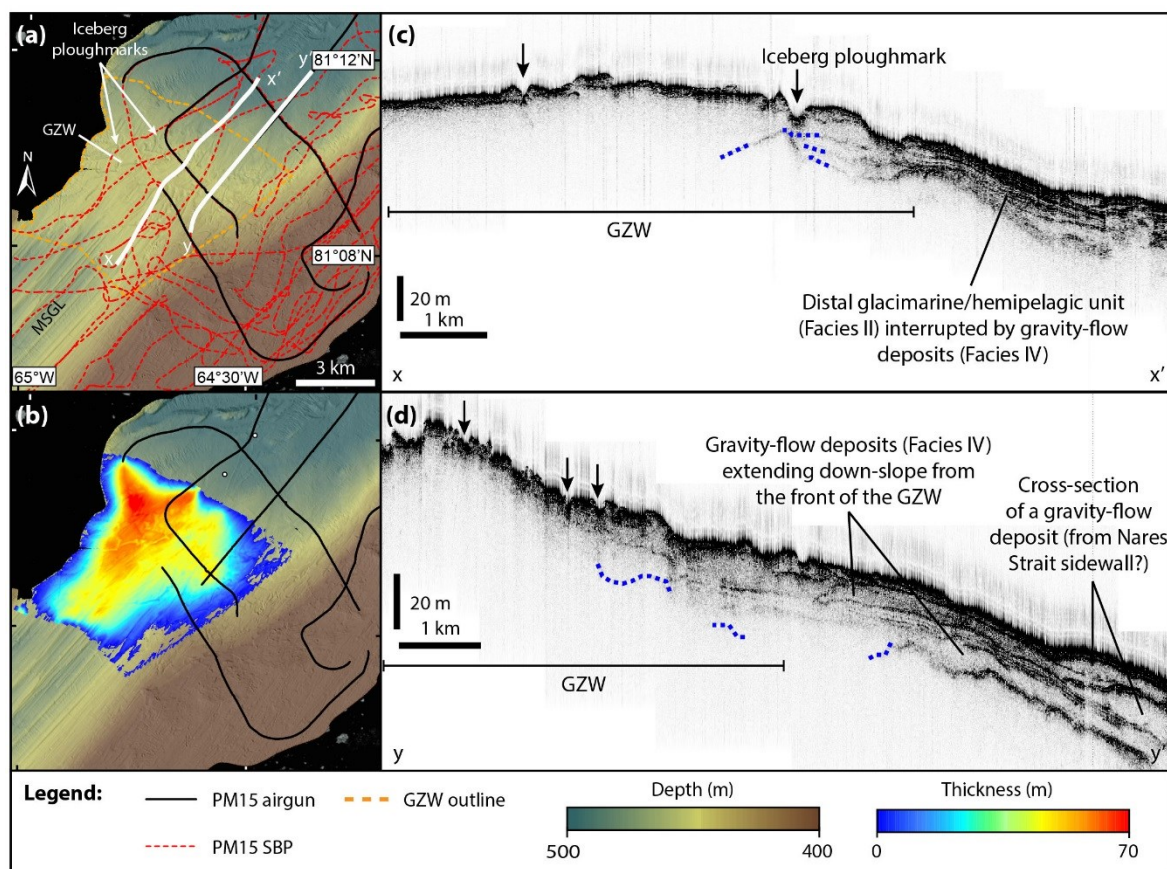
Figure 9. Mapping of the Kennedy Channel GZW. (a) AG and SBP profiles over the GZW and outline used for volume calculations. (b) Isopach map for the Kennedy Channel GZW (using a sound velocity of 1500 m s⁻¹). (c) SBP profile over the GZW showing the acoustically semi-transparent lenticular bodies (Facies IV) interfingered with acoustically stratified conformable units down slope (Facies III); location shown in (a). (d) SBP profile of the frontal part of the GZW showing semi-transparent units tapering down slope (Facies IV); location shown in (a). Black arrows point to iceberg ploughmarks; blue dashed lines show deepest sub-bottom reflections in the GZW interpreted as the base of the GZW.

940
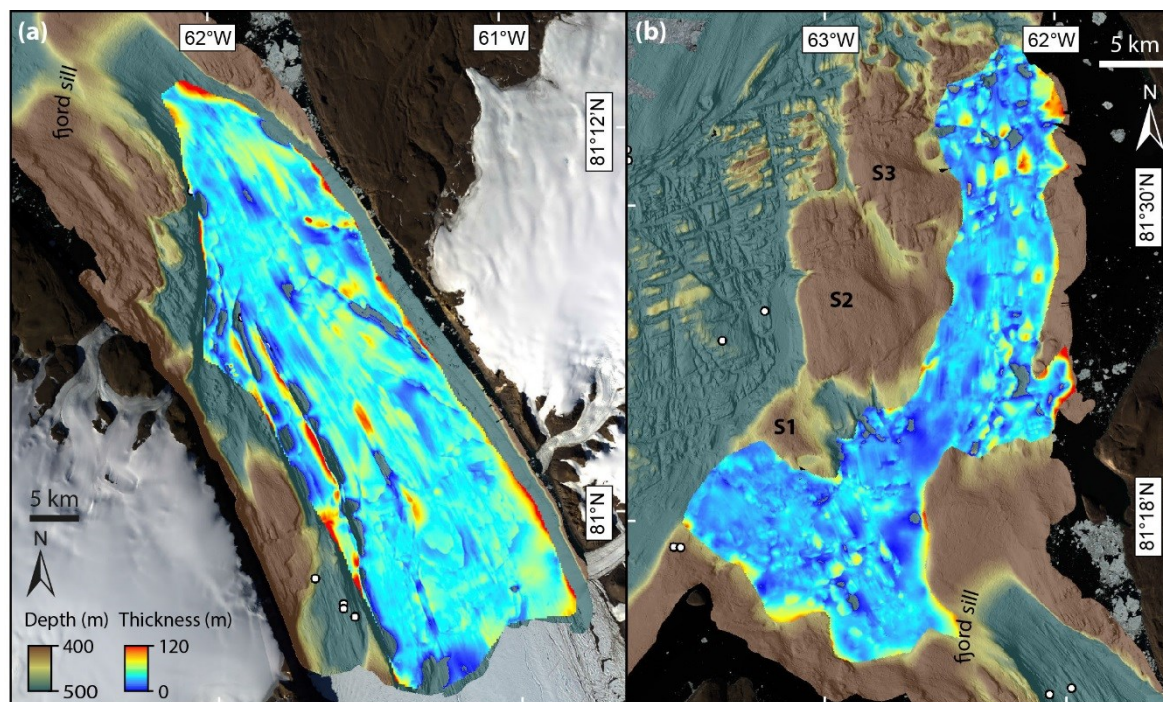
Figure 10. Isopach maps of the deglacial sediment pile for (a) Petermann Fjord, and (b) inner Hall Basin.
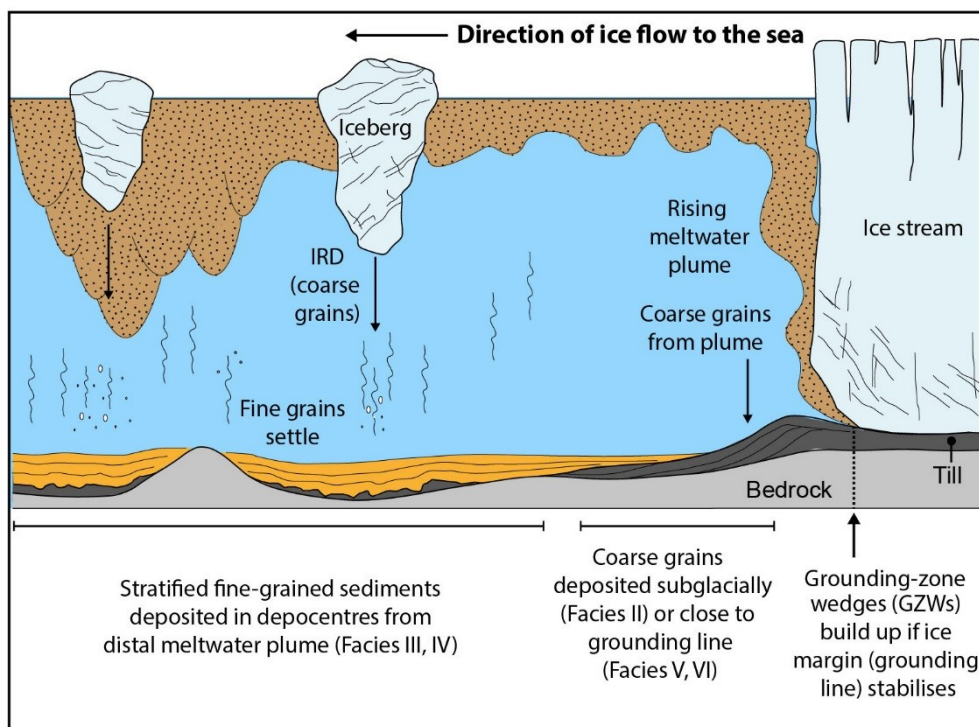
Figure 11. Processes of glaciomarine sedimentation at the marine-terminating margin of a Greenland outlet glacier (no ice shelf/tongue). The related seismo-acoustic facies as mapped in the Petermann-Nares Strait system are shown at the bottom of the figure.